1-1-2010

Overnight Atmospheric Transport and Chemical Processing of Photochemically Aged Houston Urban and Petrochemical Industrial Plume

Rahul A. Zaveri
Pacific Northwest National Laboratory

Paul B. Voss
Smith College, pvoss@smith.edu

Carl M. Berkowitz
Pacific Northwest National Laboratory

Edward Fortner
Aerodyne Research, Inc.

Jun Zheng
Texas A&M University

See next page for additional authors

Overnight atmospheric transport and chemical processing of photochemically aged Houston urban and petrochemical industrial plume

Rahul A. Zaveri,[1] Paul B. Voss,[2] Carl M. Berkowitz,[1] Edward Fortner,[3] Jun Zheng,[4] Renyi Zhang,[4] Ralph J. Valente,[5] Roger L. Tanner,[5] Daniel Holcomb,[6] Thomas P. Hartley,[7] and Leslie Baran[8]

Received 4 November 2009; revised 29 July 2010; accepted 15 September 2010; published 3 December 2010.

[1] Overnight atmospheric transport and chemical evolution of photochemically aged Houston urban and petrochemical industrial plume were investigated in July 2005. We report here on the 26 July episode in which the aged plume was tagged 1.5 h before sunset with a pair of free-floating controlled meteorological balloons, which guided quasi-Lagrangian aircraft sampling in the plume as it was advected 300 km to the north over 8 h. The aged plume around sunset was well mixed within a 1600 m residual layer, and was characterized by enhanced levels of aerosol, O_3, CO, olefins, acetaldehyde, total odd nitrogen compounds (NO_y), and relatively small amounts (<1 ppbv) of NO_x. The plume experienced appreciable shearing overnight due to the development of a low-altitude nocturnal jet between 300 and 500 m above mean sea level (MSL). However, the plume above 600 m MSL remained largely undiluted even after 8 h of transport due to lack of turbulent mixing above the jet. About 40–60% of the NO_x present in the aged plume around sunset was found to be depleted over this 8 h period. A constrained plume modeling analysis of the quasi-Lagrangian aircraft observations suggested that by dawn this NO_x was converted to nitric acid, organic nitrates, and peroxy acyl nitrates via reactions of NO_3 radicals with enhanced levels of olefins and aldehydes in the plume. Sensitivity of NO_x depletion to heterogeneous hydrolysis of N_2O_5 on aerosols was examined. These results have significant implications for the impacts of urban and industrial pollution on far downwind regions.

Citation: Zaveri, R. A., et al. (2010), Overnight atmospheric transport and chemical processing of photochemically aged Houston urban and petrochemical industrial plume, *J. Geophys. Res.*, *115*, D23303, doi:10.1029/2009JD013495.

1. Introduction

[2] Rapid ozone (O_3) formation in the Houston metropolitan area has been linked to large amounts of reactive volatile organic compounds (e.g., olefins and aldehydes) and NO_x (= NO + NO_2) emitted from petrochemical industrial facilities in the Ship Channel area east of the Houston urban center, with ozone concentrations exceeding 100 ppbv observed within 50–100 km downwind of Houston by late afternoon [*Ryerson et al.*, 2003; *Daum et al.*, 2004; *Jobson et al.*, 2004; *Kleinman et al.*, 2005; *Jiang and Fast*, 2004]. Such photochemically aged plumes containing high levels of ozone, unreacted NO_x, volatile organic compounds (VOCs), and aerosol particles can be transported overnight in the residual layer with little dilution and adversely affect the air quality of regions several hundred kilometers downwind the next day. This is a major concern for the state of Texas as well as for other regions that are close to and downwind of large petrochemical industrial facilities around the world. It is therefore of interest to understand the transport characteristics and the extent of chemical processing of O_3, NO_x, and VOCs in such concentrated pollution plumes as they are transported overnight.

[3] After sunset, the NO_2 present in the photochemically aged plume can react with O_3 to form highly reactive nitrate radicals (NO_3). Depending on the ambient temperature, NO_3

[1]Atmospheric Sciences and Global Change Division, Pacific Northwest National Laboratory, Richland, Washington, USA.
[2]Picker Engineering Program, Smith College, Northampton, Massachusetts, USA.
[3]Aerodyne Research, Inc., Billerica, Massachusetts, USA.
[4]Department of Atmospheric Sciences, Texas A&M University, College Station, Texas, USA.
[5]Environmental Technologies Department, Tennessee Valley Authority, Muscle Shoals, Alabama, USA.
[6]Electrical Engineering and Computer Sciences Department, University of California, Berkeley, California, USA.
[7]Department of Electrical and Computer Engineering, University of Massachusetts, Amherst, Massachusetts, USA.
[8]Department of Atmospheric Science, University of Wyoming, Laramie, Wyoming, USA.

0148-0227/10/2009JD013495

Table 1. List of Instruments and Measurements Performed on Board the Twin Otter Aircraft During the SETTS Field Campaign

Measurement[a]	Instrument	Principal of Operation	Modification/Analysis Method	Minimum Detection Limit[b] (ppbv)	Accuracy
NO	TEI Model 42S	Chemiluminescence	-	0.04	5%
NO_2	TEI Model 42S	Chemiluminescence	Xe lamp converter (NOAA/ARL Modified)	0.03	6%
NO_y	TEI Model 42S	Chemiluminescence	Heated molybdenum catalyst	0.04	7%
O_3	TEI Model 42S	Chemiluminescence	Operated in reversed mode for fast response	0.06	6%
CO	Aero-Laser Model AL5002	Vacuum UV fluorescence	-	0.5	4%
Aerosol size distribution: 0.1 to 0.4 μm	LASAIR particle counter	Optical counter	-	-	25%
VOCs	PTR-MS IONICON Analytik	Chemical ionization of VOCs	-	See Table 2	See Table 2
T and RH	Vaisala HMP45C	Thermistor and capacitance hygrometer	-	-	T: ± 0.3 C, RH: ± 3%
Lon, Lat, Alt	Garmin 195	GPS	-	-	Lat, Lon: ± 7 m, Alt: ± 14 m
Atmospheric pressure	Setra Systems 270B	Capacitance cell	-	-	±0.05%

[a]Raw data for all measurements except VOCs were recorded at 5 s intervals. Raw VOC data from PTR-MS were recorded at ~11 s intervals.
[b]Minimum detection limits (MDL) are for 1 min average data.

reacts rapidly and reversibly with NO_2 to form dinitrogen pentoxide (N_2O_5), which can undergo heterogeneous hydrolysis on aerosol particles to form HNO_3 [*Brown et al.*, 2006, 2009]. NO_3 radicals can also react with high concentrations of olefins and aldehydes present in the petrochemical plumes to form various products, including HNO_3, peroxy acyl nitrates (PANs), and organic nitrates [*Atkinson*, 1994]. The overall rate and efficiency with which NO_x is converted to HNO_3 and stable organic nitrates is of interest, because at dawn the residual NO_3 and N_2O_5 can photolyze or dissociate back to NO_x and subsequently produce additional O_3 in the presence of VOCs.

[4] Very few airborne studies have focused on the overnight transport and transformation of urban/industrial plumes relative to similar studies carried out during the daytime [*Brown et al.*, 2009]. Not only are the logistics of nighttime aircraft missions more difficult, but it is quite challenging to locate the same urban/industrial plumes at increasing downwind distances in the dark and hence to make measurements describing the chemical evolution as a function of increasing processing time through the night.

[5] In July 2005, Texas Environmental Research Consortium (TERC) and Houston Advanced Research Center (HARC) supported the Southeast Texas Transport Study (SETTS) field campaign to investigate the overnight transport characteristics and chemical transformation of the Houston urban and industrial plumes. We report here on the aircraft observations taken in the photochemically aged Houston urban/industrial plume as it was transported to the north on the night of 26–27 July 2005. A quasi-Lagrangian aircraft sampling strategy, guided by the newly developed controlled meteorological (CMET) balloons, was used to monitor the chemical evolution of key trace gases and aerosol in the plume at increasing downwind distances. Analysis of the CMET balloon trajectory data provided a firm basis for relating aircraft measurements taken in the aged plume just north of Houston around sunset to the measurements made 8 h later in approximately the same plume segment nearly 300 km downwind. Comparison of the aircraft observations in these "initial" and "later" plume segments showed significant loss of NO_x over this period. Constrained plume modeling analysis of the quasi-Lagrangian data provided further insights into the roles of NO_3-VOC reactions and heterogeneous hydrolysis of N_2O_5 in the conversion of NO_x into HNO_3, organic nitrates, and PAN. Potential impacts of such an aged plume on the next-day photochemical production of O_3 are briefly discussed.

2. Field Experiment

[6] The base of operations for the SETTS campaign was the Lone Star Executive Airport, near Conroe, Texas, just north of the greater Houston area. A Twin Otter aircraft was deployed to study three overnight plume transport episodes on 21, 23, and 26 July 2005. Each episode consisted of three aircraft flights. The first flight was conducted over and around the Houston urban and Ship Channel areas during late afternoon to early evening period. The second and third flights were conducted at increasing downwind distances from Houston, with the last flight ending at early morning hours the next day. *Luria et al.* [2008] presented an analysis for the 21 July episode. In this study, we focus on the 26

July episode. The findings and conclusions of the Luria et al. study are briefly contrasted with the present work in section 4.

2.1. Twin Otter Aircraft Instrumentation

[7] A DeHavilland Twin Otter fixed-wing aircraft (Model DHC-6-300) was leased from Twin Otter International Ltd, and was outfitted with a suite of instruments to measure mixing ratios of several trace gases, aerosol size distribution, Global Positioning System (GPS) location, temperature, pressure, and relative humidity. A complete list of measurements, instruments, minimum detection limit, and measurement accuracy is given in Table 1. The Environmental Technologies Department of the Tennessee Valley Authority (TVA) deployed several trace gas analyzers manufactured by Thermo Environmental Instruments (TEI), Inc., Franklin, MA. These included an Aero-Laser Model AL5002 vacuum UV fluorescence CO analyzer and three Model 42S chemiluminescence instruments that were modified to measure O_3, NO, NO_2. While SO_2 was also measured with a TEI Model 43S instrument, the data were not used in this study because the instrument suffered from an unresolved problem which caused it to be much slower (~1 min) than normal operation. A Model 42S system with heated (325°C) molybdenum catalyst converter was used to measure NO_y (= sum of all gaseous and particulate odd nitrogen oxide species) as described in detail by *Tanner et al.* [1998]. The molybdenum catalyst converter was placed directly adjacent to the inner skin of the aircraft and the inlet length was kept at a minimum to reduce the residence time inside the inlet to less than 0.05 s. This configuration greatly reduced the loss of nitrates and other species in both the gas and particle phases to the inlet wall, although the actual inlet transmission efficiencies were not measured. Once daily, when the aircraft was on the ground, the molybdenum converters were baked at 500°C while zero air was fed through them. This process helped remove residual material from the converter mesh and maintained the NO_y conversion efficiency at 95–99%. The bake-out process also helped reduce the baseline noise during flight. The conversion efficiency for the NO_2 photolysis cell was determined on a daily basis, so that any gradual reduction in efficiency as the lamp aged could be incorporated in the data reduction process. Inlet filters on the instruments were replaced with low dead volume filters to improve the time response. The mixing ratios of NO_x and NO_z were calculated as $NO_x = NO + NO_2$ and $NO_z = NO_y - NO_x$, respectively.

[8] Response time of the gas analyzers to reach 90% of the signal was less than 5 s. The raw data from the above mentioned trace gas analyzers were recorded at 5 s intervals, and ~1 min average data were used for the analysis presented in this study. Additional details regarding the performance of trace gas analyzers, the sampling manifold, the calibration procedures, and the data system are given by *Valente et al.* [1998] and *Luria et al.* [1999, 2000].

[9] Selected volatile organic compounds (VOCs) were measured by a compact Proton Transfer Reaction Mass Spectrometer (PTR-MS), which was installed and operated by Texas A&M University. The operating and data processing procedures were the same as those used during its deployment in Mexico City during the MILAGRO 2006 campaign as given by *Fortner et al.* [2009]. Its working principle has been detailed by *Hansel et al.* [1995] and *Lindinger et al.* [1998]. The PTR-MS utilizes hydronium ions (H_3O^+) to ionize VOCs through proton transfer reactions under kinetically limited condition ($[H_3O^+] >> [\text{product ions}]$). Hydronium ion concentration was indirectly obtained from the measurement of its isotope peak of $H_3^{18}O^+$ at *m/z* 21. The concentration of a VOC was calculated according to

$$[\text{VOC}] = [\text{VOCH}^+]/kt[\text{H}_3\text{O}^+], \quad (1)$$

where $VOCH^+$ is the protonated VOC, k is the proton-transfer reaction rate constant, and t is the reaction time inside the drift tube. Further calibrations with pure VOC standards were applied to correct errors introduced by mass transmission efficiency and uncertainties introduced by the rate constants taken from literature.

[10] Throughout all flights, the inlet flow rate was regulated by a pressure controller, which was set to 350 hPa that maintained the PTR-MS drift tube pressure at 1.98 hPa. An E/N ratio of 115 Townsend (1 Td = 10^{-17} V cm^2 molecule^{-1}) was utilized, where E is the electric field strength in V cm^{-1} and N is the number concentration of the buffer gas in molecule cm^{-3}. Although water clusters of hydronium ion (i.e., $H_3O^+(H_2O)_{n=1,2}\ldots$) can undergo similar proton-transfer reactions with some VOCs having a proton affinity higher than that of $H_3O^+(H_2O)_n$, under the experimental conditions used in this work, $H_3O^+(H_2O)_{n=1}$ (*m/z* 37) was found to vary between 5 to 7% of the primary H_3O^+ reagent ion and its effects on VOC concentrations was accounted for in calibrations.

[11] During most flights the reagent ion isotope of H_3O^+ was measured at mass to charge ratio (*m/z*) 21 along with a suite of 5 product ions (*m/z* = 43, 45, 57, 69 and 71) sampled sequentially by the PTR-MS. Each product ion was monitored for 2 s so that the time between samples was approximately 11 s. Spectral scans from *m/z* 21–250 were also conducted periodically (at least once during each flight) to survey mass peaks that might have been missed while in the single ion scan mode. However, no other VOC species with significant concentration was detected during the spectral scan mode measurements. Background checks were conducted using zero air approximately hourly. The background signals were subtracted from the raw data before converting them into mixing ratios. Calibrations were conducted at the conclusion of each flight and calibration correction factors were determined. Calibrations of the PTR-MS were conducted using a custom mix calibration gas cylinder (Spectra Gas) containing propene, acetaldehyde, *cis*-2 butene, isoprene, benzene, toluene and m-xylene, and mixing ratios were typically varied from 2 to 20 ppbv. The data presented in this paper are ~1 min averages.

[12] The signal at *m/z* 45 is uniquely attributed to acetaldehyde (CH_3CHO) [*Warneke et al.*, 2003], although a minor interference from CO_2 is possible, with 1 ppmv CO_2 equivalent to 1 pptv acetaldehyde [*Rogers et al.*, 2006]. However, this interference does not pose a problem in the present study, because the zero air used in this work contained CO_2 at a similar level as in the ambient air. The signal at *m/z* 43 can be from propene, cyclopropane, and a number of VOCs such as butenes, pentenes, acetic acid,

Table 2. List of VOCs Measured by the PTR-MS

m/z	Primary Species	Interferences	Minimum Detection Limit[a] (ppbv)	Accuracy (%)
43	propene	cyclopropane, 2-propanol,butenes, pentenes, acrolein, acetic acid, ethyl acetate	0.55	35
45	acetaldehyde	none	0.5	35
57	butenes	acrolein, butanol	0.13	35
69	isoprene	cyclopentene, pentanal, 2 methyl-3-buten-2-ol	0.035	20

[a]Minimum detection limits (MDL) are for 1 min average data.

acrolein, and heavier acetates which fragment to *m/z* 43. The intercomparison between PTR-MS and GC-FID during TexAQS 2000 campaign indicated that *m/z* 43 mixing ratios above a certain threshold (5–10 ppbv) in the Houston Ship Channel region were dominated by propene [*Karl et al.*, 2003; *Kuster et al.*, 2004]. The signal at *m/z* 57 is generally regarded to include the sum of butenes, acrolein, and butanol [*Karl et al.*, 2003; *Warneke et al.*, 2003]. The signal at *m/z* 69 is primarily attributed to isoprene with possible contributions from 2-methyl-3-buten-2-ol, pentanal, methyl butanal, and pentenol [*Fall et al.*, 2001; *de Gouw et al.*, 2003; *Warneke et al.*, 2003]. The signal at *m/z* 71 includes the sum of methyl vinyl ketone, methacrolein, pentenes, and methyl butene [*Warneke et al.*, 2003]. Table 2 summarizes the primary and interfering species associated with each *m/z* and its minimum detection limit.

[13] Finally, Battelle Northwest Laboratories provided a Lasair aerosol particle sizer to measure size distribution between 0.1 and 0.4 μm. The raw data were recorded every 5 s, and 1 min average data were used in the analysis. The 1 min average aerosol, O_3, CO, NO_x, NO_y, and NO_y* and all ancillary data were linearly interpolated to the PTR-MS time base.

2.2. Controlled Meteorological Balloons

[14] Constant-altitude balloons have been extensively used to study low-level atmospheric wind patterns and air pollution dispersion [*Angell et al.*, 1976; *Zak*, 1981; *Reisinger and Mueller*, 1983] and to guide Lagrangian aircraft measurements in several field campaigns including ASTEX [*Zhuang and Huebert*, 1996], ACE-1 [*Suhre et al.*, 1998], ACE-2 [*Johnson et al.*, 2000], ICARTT [*Riddle et al.*, 2006], and NAOPEX [*Zaveri et al.*, 2010]. In this study, we used the controlled meteorological (CMET) balloons [*Voss et al.*, 2005] for in situ characterization of the evolution of chemical and meteorological variables in the residual layer as the pollutants contained within it were advected downwind overnight. The CMET balloons are altitude-controlled platforms with bidirectional satellite communication and long-duration flight capability. Once airborne, these balloons can be commanded to perform soundings as they drift with the mean flow over periods ranging from several hours to multiple days. The resulting profiles of winds, temperature, pressure, and water vapor provide a unique view of the evolving structure of the atmosphere. The CMET balloons also serve as physical markers to locate the plume at increasing downwind locations.

[15] The CMET balloons are small (0.9 m diameter × 2 m tall) and easily transportable in a minivan and can be launched from any open site (Figure 1). Each balloon carried a 400 g payload consisting of an aspirated temperature and humidity sensor (Vaisala model 17204HM, ±5% RH, ±1°C), a satellite modem (Iridium model A3LA-I), and a pump valve system for altitude control. Position was measured by a GPS receiver (Synergy Systems model M12+, ±5 m horizontal, ±50 m vertical) with short-term vertical resolution increased to ±0.2 m by a pressure altimeter (Motorola model MPX 5100AP, ±25 mbar).

[16] All balloon flights were closely coordinated with the Federal Aviation Administration (FAA) and Air Traffic Control (ATC). The balloon-based measurements were made at 15 s intervals during soundings and at 30 s intervals during horizontal float mode. CMET balloon position data were continuously transmitted to the base of operations and to the Twin Otter aircraft via satellite communication. The CMET balloon data received onboard the Twin Otter was

Figure 1. A pair of two CMET balloons just before launch from an open site north of Houston.

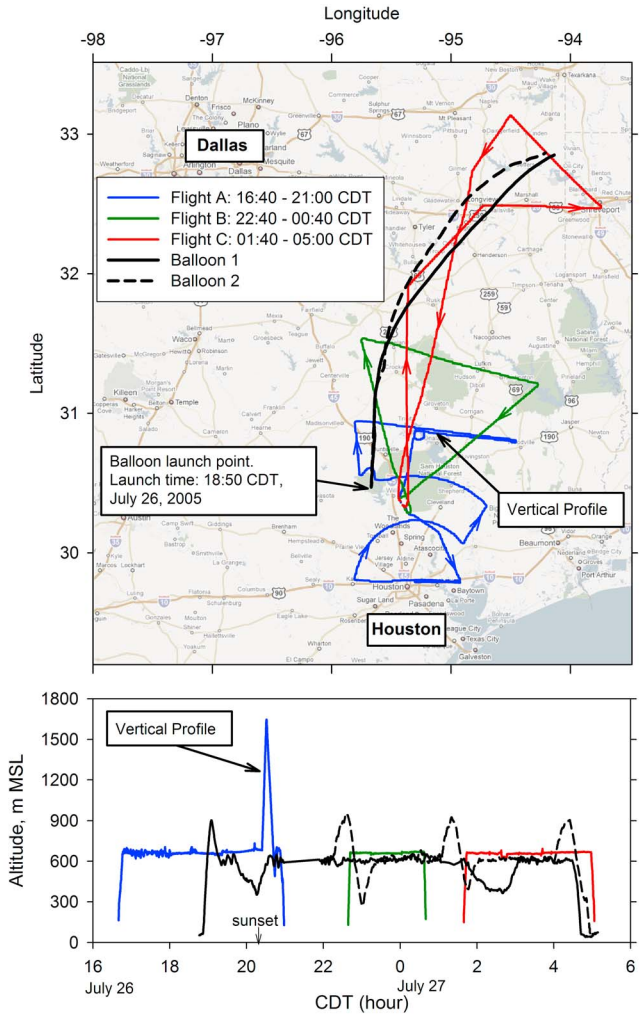

Figure 2. Flight paths and altitudes for the three aircraft flights and the two CMET balloon trajectories on 26–27 July 2005.

fed into a customized aircraft flight planning software, which was used to guide the aircraft transects in the vicinity of the CMET balloons as they drifted downwind. The resulting quasi-Lagrangian observations readily lend themselves to constrained plume modeling (CPM) analysis and interpretation using a detailed Lagrangian gas-aerosol chemistry model.

3. The 26 July Episode Observations

3.1. Evidence for Mixed Urban and Petrochemical Industrial Plumes

[17] Here we focus on the observations made in the Houston urban and petrochemical industrial plume on 26–27 July 2005. Figure 2 shows the flight paths and altitudes for the three aircraft flights and trajectories of the two CMET balloons for the 26 July episode. Sampling for the 26 July episode began with a late afternoon (1640 central daylight time or CDT (local time)) aircraft flight (Flight A) to identify the location of the Houston urban and petrochemical industrial plumes. During Flight A, the aircraft made one transect over the Ship Channel and the urban center, followed by three more at increasing downwind distances to the north until 2100 CDT. A vertical profile between 675 and 1650 m MSL was also performed during the last transect as indicated on the map. As shown in Figure 3, O_3 mixing ratios were lowest (20–30 ppbv) over the Ship Channel while significantly higher (up to 100 ppbv) in the aged air to the north during Flight A. CO mixing ratios were close to the background levels (80–100 ppbv) over the Ship Channel, but more than 180 ppbv in the photochemically aged air to the north, which had passed over the urban area earlier that day. On the other hand, NO_y mixing ratios were more than 10 ppbv over the Ship Channel while about 6–8 ppbv in aged air to the north. As expected, the NO_x/NO_y ratios were >0.6 over the Ship Channel and urban center areas and close to 0.2 in the aged air to the north. Moderate CO levels and high NO_y levels together with high NO_x/NO_y ratios observed over the Ship Channel are consistent with the fresh emissions from petrochemical industrial facilities [*Ryerson et al.*, 2003]. Relatively higher levels of both CO and NO_y observed to the north of Ship Channel during Flight A are indicative of vehicular urban emissions that have mixed with emissions from petrochemical industrial facilities. As shown in Figure 4, relatively uniform vertical profiles of O_3, CO, NO_x, and NO_y mixing ratios, with sharp decreases at 1650 m MSL, observed in the last transect during Flight A indicate that the photochemically aged plume was well mixed in the ~1600 m high residual layer at sunset (2018 CDT).

[18] Based on the real-time O_3, CO, and NO_y data accessed onboard the aircraft during Flight A, the location of the Houston plume was estimated and a decision was made to launch a pair of CMET balloons at 1850 CDT to place the balloons close to the photochemically aged plume segment observed about 100 km north of the Ship Channel. The altitude of the balloons were stabilized at ~600 m above mean sea level (MSL), high enough for the aircraft to safely fly at night and but low enough to sample the aged plume. Also, one balloon was programmed to perform soundings of ±300 m around the nominal float altitude of 600 m MSL approximately once every 2 h while the other remained relatively steady at the float altitude.

[19] The second aircraft flight (Flight B) started at 2240 CDT to make one transect in the vicinity of the balloons, which were then farther north of the previous transect, in order to sample the plume again. The aircraft returned to the airport at 0040 CDT (27 July) for refueling and took off again for the third and final flight (Flight C) at 0140 CDT. The balloons had been advected nearly 300 km to the north when the aircraft caught up with them around 0310 CDT to locate and make the final transects within the mixed Houston urban and petrochemical industrial plume. Peak ozone levels of up to ~100 ppbv, with background values of ~20–30 ppbv, were observed again at this time.

[20] As shown in Figure 5, the mixing ratios of PTR-MS masses *m/z* 43 and 45 tracked with NO_y mixing ratios in all three flights. Mixing ratios of *m/z* 69 (isoprene) and *m/z* 71 (methyl vinyl ketone + methacrolein + pentenes) were frequently below their detection limits (hence not shown). Figure 6 shows the scatterplots of *m/z* 43 and 45 versus NO_y. The *m/z* 43 to NO_y ratios mostly ranged between 0.5 and 2, which are consistent with the reported propene/NO_x

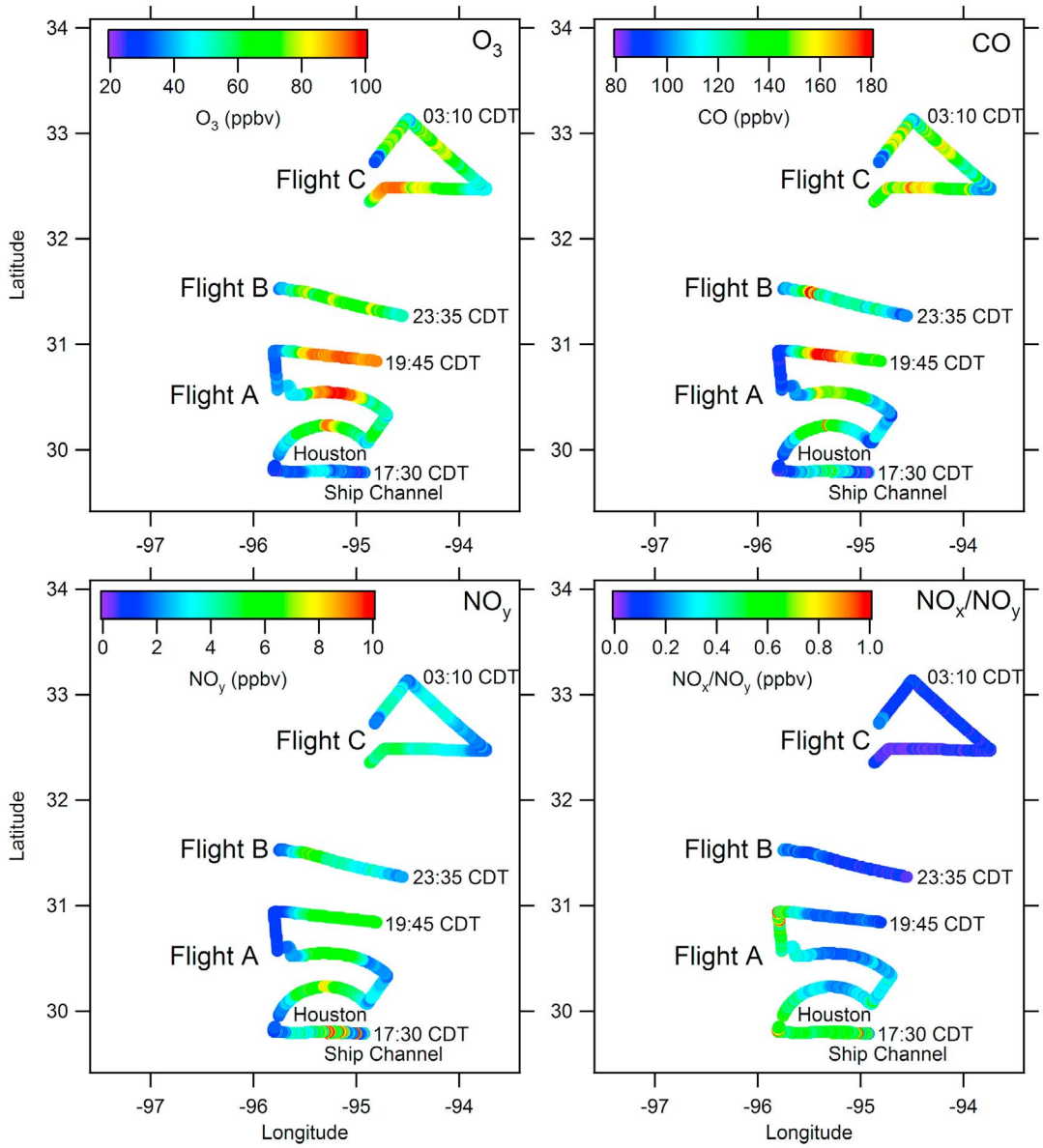

Figure 3. Spatial distributions of O_3, CO, NO_y mixing ratios, and NO_x/NO_y ratio along the aircraft flight paths. Only selected flight segments are shown for clarity. Mean local times are indicated next to select transects.

emission ratios for various petrochemical complexes along the Ship Channel [*Ryerson et al.*, 2003]. The large scatter in the *m/z* 43 versus NO_y plot may also arise due to mixing of propene and NO_x from petrochemical industrial sources with NO_x from urban/vehicular sources. The weak but distinct correlation (R^2 = 0.4) between *m/z* 45 (i.e., acetaldehyde) and NO_y is reasonable since photooxidation of propene as well as many other urban VOCs leads to the formation of acetaldehyde. The presence of high concentrations of NO_y, olefins, and acetaldehyde over the Ship Channel as well as to the north together with high concentrations of CO indicates that petrochemical industrial emissions had mixed with urban emissions. While there are anthropogenic sources of isoprene in the Houston Ship Channel [*Gilman et al.*, 2009], very low *m/z* 69 mixing ratios found during this study suggest that the observed signal was likely of biogenic origin.

3.2. Overnight Transport Characteristics

[21] The fact that peak ozone concentrations seen during Flight A were preserved in Flight C suggests that very little dilution occurred in the polluted air parcel sampled twice at ~670 m MSL. Vertical shearing occurred due to the development of a low-altitude nocturnal jet below the nominal aircraft flight altitude for this study. The development of this jet between 300 and 500 m MSL can be seen from the time evolution of wind speed and direction, potential temperature, and specific humidity profiles measured by the two CMET balloons (Figure 7). The wind speeds between 300 and 500 m MSL around 1700 CDT were about 7 m s^{-1}, but by 2200 CDT they had increased to more than 12 m s^{-1}. The

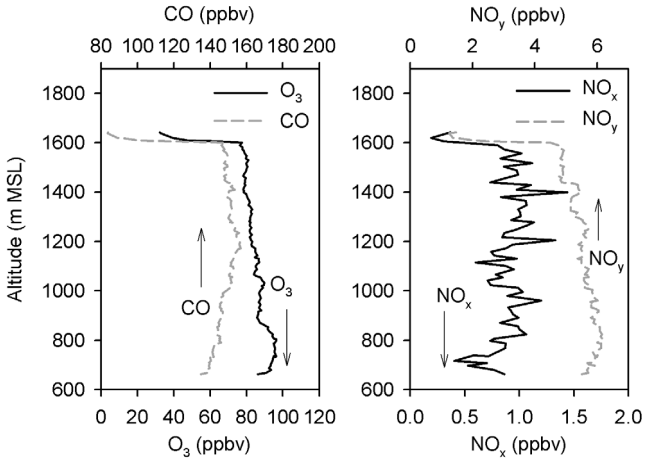

Figure 4. Vertical profiles of O_3, CO, NO_x, and NO_y mixing ratios during Flight A. The arrows indicate the corresponding x axes for each profile.

increased wind speeds between 300 and 500 m MSL coincided with lower potential temperatures and moister air that was likely advected inland from the Gulf of Mexico.

[22] While the low-level jet transported significantly more humid air from south, a barrier to mixing at 600 m MSL appears to have persisted throughout the duration of the night, with almost no dilution of the residual layer above the jet. Local gradients in the observed wind velocity and virtual potential temperature profiles were used to estimate the gradient Richardson number, which is a dimensionless ratio of the buoyant production or consumption of turbulence to the shear production of turbulence [*Stull*, 1988]:

$$\mathrm{Ri} = \frac{\frac{g}{T_v}\frac{\partial \theta_v}{\partial z}}{\left(\frac{\partial U}{\partial z}\right)^2 + \left(\frac{\partial V}{\partial z}\right)^2}, \qquad (2)$$

where θ_v is the virtual potential temperature, T_v is the virtual absolute temperature, z is the altitude, g is the gravitational acceleration, and U and V are the east-west and north-south wind components, respectively. The flow is dynamically unstable and turbulent when $\mathrm{Ri} < 0.25$ and tends to be stable and laminar for $\mathrm{Ri} > 0.25$. Calculation of derivatives of wind velocity and virtual potential temperature with respect to altitude from balloon soundings tend to be rather noisy [*Stull*, 1988]. However, a clear pattern emerges when the median values of many individual measurements ($10 < n < 100$) at each altitude from multiple soundings are plotted as a function of altitude as shown in Figure 8. A distinct peak at 600–800 m, with values greater than unity suggests the flow was laminar in this layer. This result is consistent with the lack of upward mixing above the jet as seen in specific humidity profiles.

[23] Trajectories computed at different altitudes from the balloon wind profiles support this general interpretation of transport downwind of Houston on July 26 (Figure 9). Trajectories at altitudes encompassing the balloon soundings (350–800 m MSL) show that the air mass sheared and accelerated below 600 m MSL. At the altitude of the aircraft flights (approximately 50 m above the balloons), wind velocity was uniform with altitude, with virtually no shearing. The measurements from the CMET balloons thus present a self-consistent picture: a low-altitude nocturnal jet formed below 600 m MSL, which brought cooler and more humid air below the nominal balloon and aircraft flight altitudes. The temperature gradient that developed as a result created a strong inversion and barrier to vertical mixing which confined the turbulent mixing to altitudes below 600 m MSL. Above this altitude, the mixed Houston urban and petrochemical industrial plume remained largely intact as it was transported 300 km to the north overnight.

3.3. Evidence for Chemical Processing

[24] Based on the CMET balloon trajectory analysis it was determined that the fourth transect (i.e., the east-west segment close to the 31 degree latitude) during Flight A corresponded to the air parcels sampled between 32 degree and 33 degree latitudes during Flight C 8 h later. Figure 10 shows these segments of Flights A and C paths along with

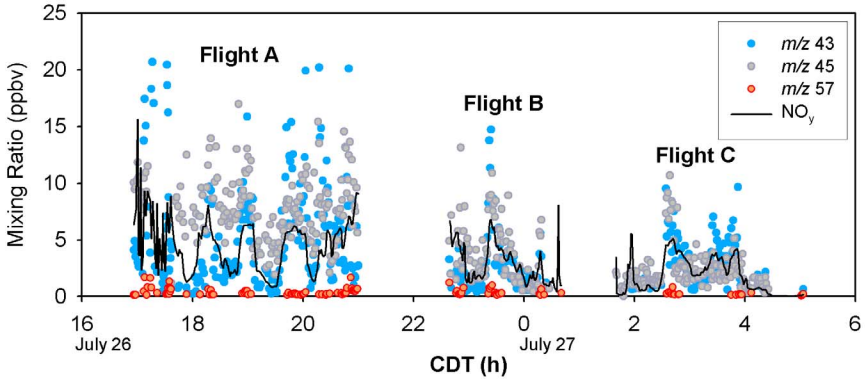

Figure 5. Time series of NO_y and PTR-MS masses *m/z* 43, 45, and 57 during the three aircraft flights on 26–27 July 2005. Mass *m/z* 45 is uniquely attributed to acetaldehyde (CH_3CHO), while mass *m/z* 43 in Houston area is thought to be dominated by propene (C_3H_6), with minor contributions from cyclopropane, 2-propanol, and fragments of pentenes, acetic acid, and heavier acetates. Mass *m/z* 57 in Houston area is thought to be dominated by butenes (C_4H_8), with minor contributions from acrolein and butanol.

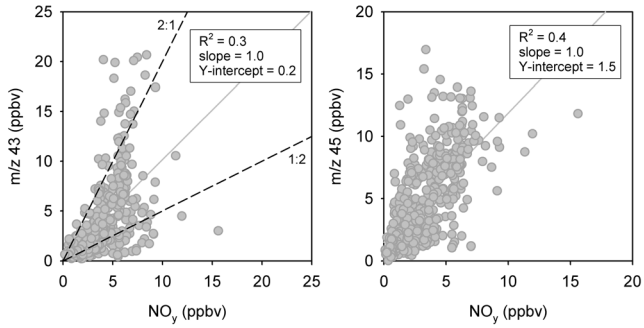

Figure 6. Scatterplots of *m/z* 43 versus NO_y and *m/z* 45 versus NO_y.

the calculated location of Segment A after advection for 8 h using CMET balloon-based wind data. Segments A and C thus represent roughly the same air parcels in the Houston plume as sampled by the aircraft in the Lagrangian sense. However, they are referred to as quasi-Lagrangian because the measurements were not made in precisely the same air parcels. Evidence for this claim can be found in Figure 11, which shows scatterplots of O_3 versus CO and NO_y versus CO for the two plume segments. These scatterplots have very similar linear regression fit parameters for Segments A and C. The slopes and *y* intercepts for linear fits of ozone versus CO are identical for the two segments. For NO_y versus CO, the difference in the slopes between Segments A and C is 12% while the difference in the *y* intercept is 15%. These results along with the trajectory analysis strongly suggest that the plume Segments A and C are quasi-Lagrangian.

[25] Figure 12 shows the scatterplots of NO_x versus NO_y and NO_z versus NO_y for the two plume Segments A and C. The NO_x/NO_y ratio decreased from 0.1 in Segment A to 0.01 in Segment C and the corresponding NO_z/NO_y ratio increased from 0.9 in Segment A to 0.99 in Segment C. The potential roles of NO_3-VOC reactions and heterogeneous hydrolysis of N_2O_5 in the observed nighttime oxidation of NO_x to NO_z (from Segment A to C) are further investigated with a constrained plume modeling approach.

4. Constrained Plume Modeling Analysis

[26] In this section we examine the overall rate and efficiency with which NO_x is converted to HNO_3 and stable organic nitrates in the nocturnal, mixed Houston urban and petrochemical industrial plume. A quantitative understanding of these nighttime chemical transformations is of practical importance, because at dawn the residual NO_3, N_2O_5 and PAN can decompose back to NO_x and subsequently produce O_3 in the presence of highly reactive olefins, aldehydes, and other VOCs. As discussed earlier, one of the

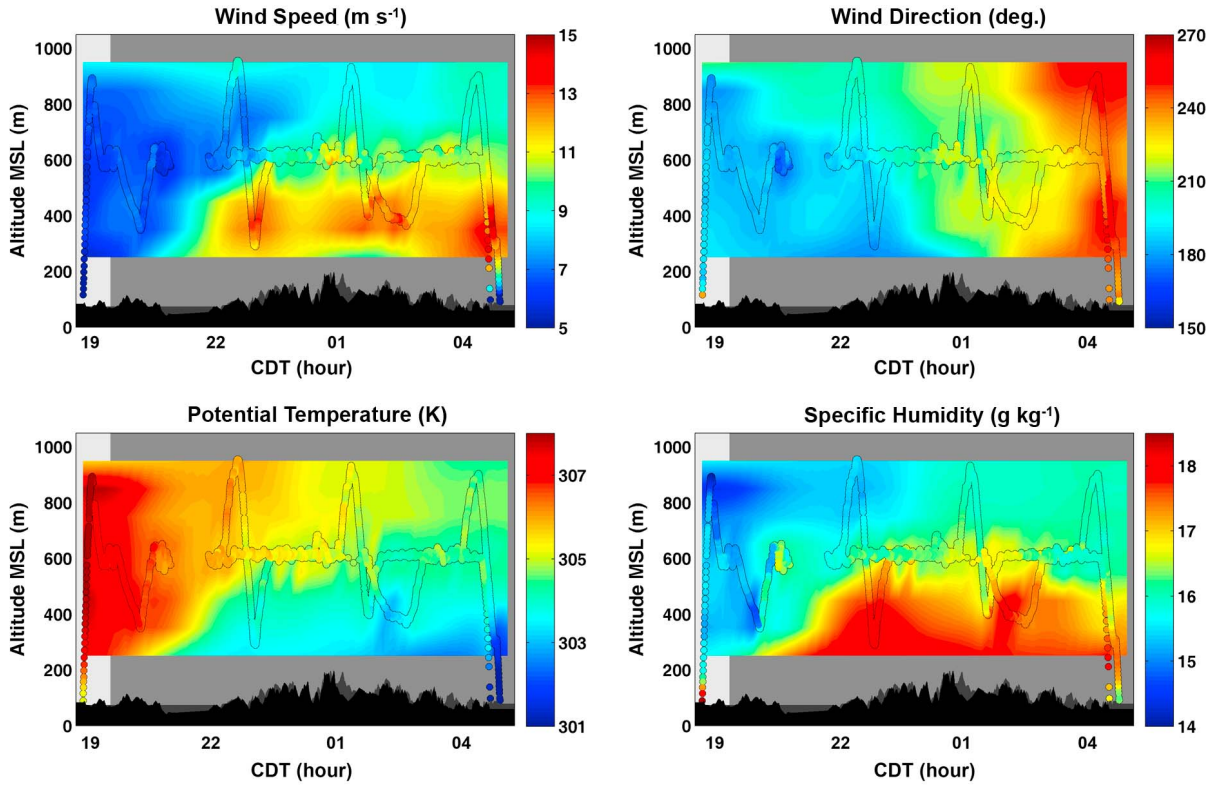

Figure 7. Evolving profiles of wind speed and direction, potential temperature, and specific humidity as measured by paired balloons during the 26 July episode. The nighttime period is denoted by the dark gray background. Black shading at the bottom is the terrain. The observed values are superimposed on interpolated surfaces. Evolution of a low-altitude nocturnal jet can be seen from the increased wind speeds between 300 and 500 m MSL starting around 2200 CDT (local time).

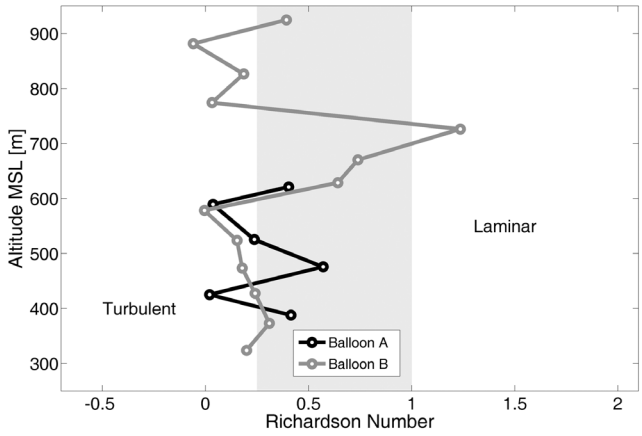

Figure 8. The gradient Richardson number calculated using sounding data from the two CMET balloons shows a strong barrier to mixing at 600–800 m MSL. The clear pattern evident here is the result of plotting the median of many individual measurements ($10 < n < 100$) at each altitude.

key reactions for converting NO_x to HNO_3 at night is the heterogeneous hydrolysis of N_2O_5 on wet aerosol surface. The homogeneous gas-phase reaction of N_2O_5 with H_2O vapor to form HNO_3 is thought to be negligibly slow [*Brown et al.*, 2009]. The other major pathway responsible for converting NO_x to HNO_3 and organic nitrates at night is via reactions of NO_3 radicals with olefins and aldehydes. Only the reactions most pertinent to the present discussion are given below [*Zaveri and Peters*, 1999; *Brown et al.*, 2003],

$$O_3 + NO \rightarrow NO_2 + O_2, \tag{3}$$

$$O_3 + NO_2 \rightarrow NO_3 + O_2, \tag{4}$$

$$NO_3 + NO_2 \rightleftharpoons N_2O_5, \tag{5}$$

$$N_2O_5 \xrightarrow[het]{\gamma(N_2O_5)} 2HNO_3, \tag{6}$$

$$NO_3 + \text{olefins} \rightarrow \text{NAP} \rightarrow \text{ONIT}, \tag{7}$$

$$NO_3 + HCHO \rightarrow HNO_3 + HO_2 + CO, \tag{8}$$

$$NO_3 + RCHO \rightarrow RC(O)O_2 + HNO_3, \tag{9}$$

$$RC(O)O_2 + NO_2 \rightleftharpoons \text{PAN}, \tag{10}$$

$$RC(O)O_2 + NO_3 \rightarrow RO_2 + NO_2, \tag{11}$$

$$RO_2 + NO_3 \rightarrow RO + NO_2 + O_2, \tag{12}$$

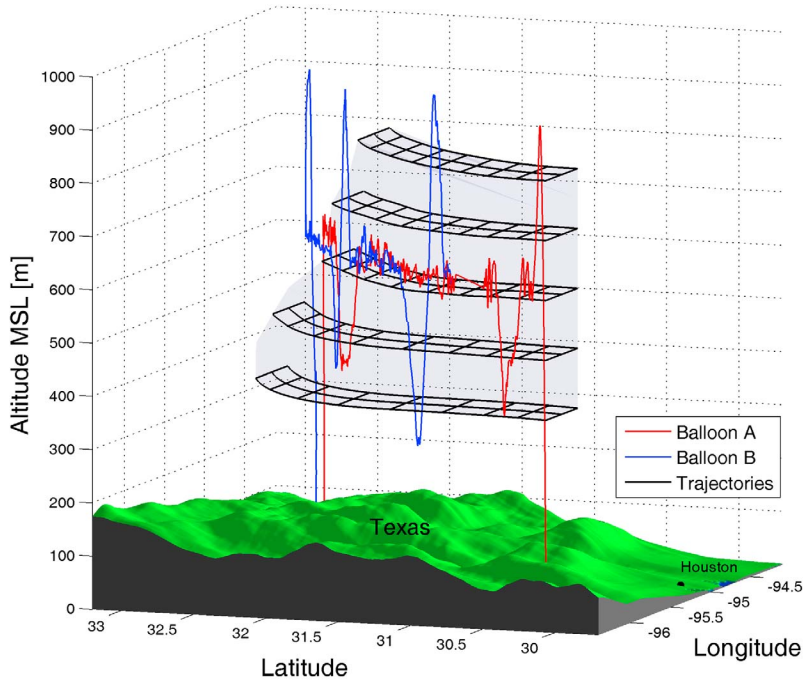

Figure 9. Trajectories derived from the interpolated wind fields shown in Figure 7. Trajectories below 600 m MSL are farther north than those above 600 m MSL for the same transport time period, indicating that the air mass accelerated and sheared due to a low-level jet below 600 m MSL. At the altitude of the aircraft flights (~50 m above the balloons, not shown here), wind velocity was uniform with altitude with virtually no shearing.

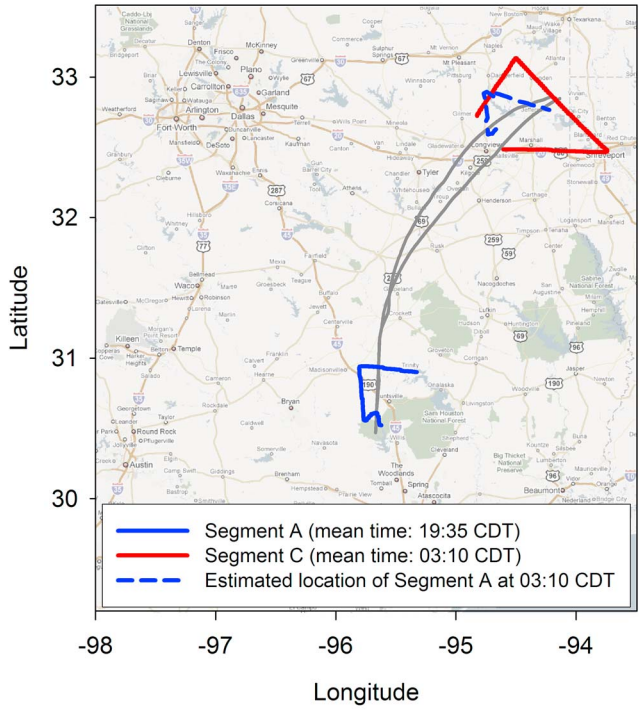

Figure 10. Selected plume segments along Flights A (blue) and C (red), which represent roughly the same air parcels in the photochemically aged, mixed Houston urban and petrochemical industrial plume as sampled by the aircraft in a quasi-Lagrangian sense. The two CMET balloon trajectories are shown with dark gray lines.

$$RO + O_2 \rightarrow HO_2 + R_{-H}O, \quad (13)$$

$$NO_3 + HO_2 \rightarrow 0.3HNO_3 + 0.7(OH + NO_2), \quad (14)$$

$$O_3 + HO_2 \rightarrow OH, \quad (15)$$

$$NO_2 + OH \rightarrow HNO_3, \quad (16)$$

where RCHO = higher aldehydes (including acetaldehyde), NAP = β-nitratoalkyl peroxy radicals, ONIT = organic nitrates (including alkyl nitrates). $RC(O)O_2$ are the generic acyl peroxy radicals that can rapidly and reversibly react with NO_2 to form peroxy acyl nitrates (PAN). RO_2 are the generic alkyl peroxy radicals. Reactions of olefins and HO_2 with O_3 are also nighttime sources of low levels of OH radicals, which can react with NO_2 to form relatively small amounts of HNO_3. The complete list of gas-phase reactions considered in the modeling study is given in *Zaveri and Peters* [1999].

[27] The N_2O_5 uptake coefficient $\gamma(N_2O_5)$ in equation (5) is a reaction probability, which is defined as the fraction of gas-particle collisions of one molecule of gaseous N_2O_5 that results in net hydrolysis to produce 2 molecules of HNO_3 [*Jacob*, 2000]. Laboratory studies of N_2O_5 uptake on various inorganic and organic aerosols have shown values for $\gamma(N_2O_5)$ ranging from < 0.001 to 0.002 at low RH and as high as 0.03 at moderately high RH (50–70%) [*Thornton et al.*, 2003; *Bertram and Thornton*, 2009]. Reductions in $\gamma(N_2O_5)$ by a factor of 3 to more than an order of magnitude were observed when certain organic coatings were present on inorganic particles [*Folkers et al.*, 2003; *Thornton and Abbatt*, 2005; *Badger et al.*, 2006; *McNeill et al.*, 2006]. Recently, *Brown et al.* [2009] estimated rather small values for $\gamma(N_2O_5)$ in the range of 0.5–6 × 10^{-3} from constrained steady state (CSS) analysis of nighttime aircraft measurements of ozone, nitrogen oxides, and aerosol surface area made in and around Houston during the 2006 TexAQS II field campaign. They also determined first-order NO_3 loss rate coefficients from the CSS analysis as well as based on the VOC measurements from canister samples.

[28] Here we carry out a constrained plume modeling (CPM) analysis of quasi-Lagrangian aircraft measurements

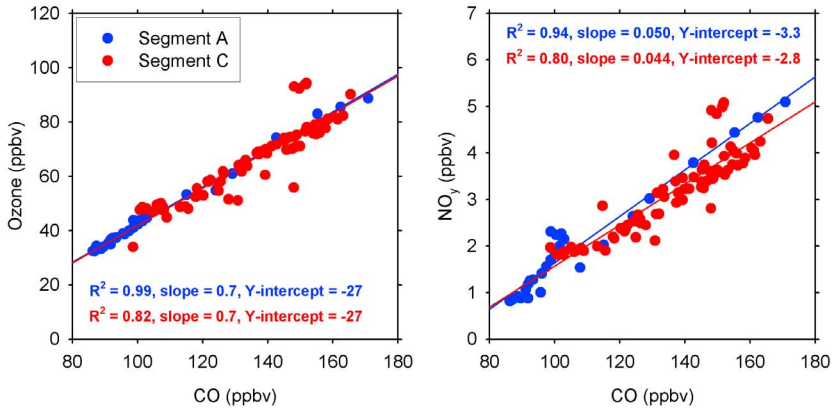

Figure 11. Scatterplots of various species for the selected plume segments A and C shown in Figure 10. Also shown on each plot are the linear regression fit parameters for the two segments. The slopes and y intercepts for linear fits of ozone versus CO are identical for the two segments. For NO_y versus CO, the difference in the slopes between segments A and C is 12% while the difference in the y intercept is 15%. These results along with the balloon trajectory analysis suggest that the plume segments A and C are quasi-Lagrangian.

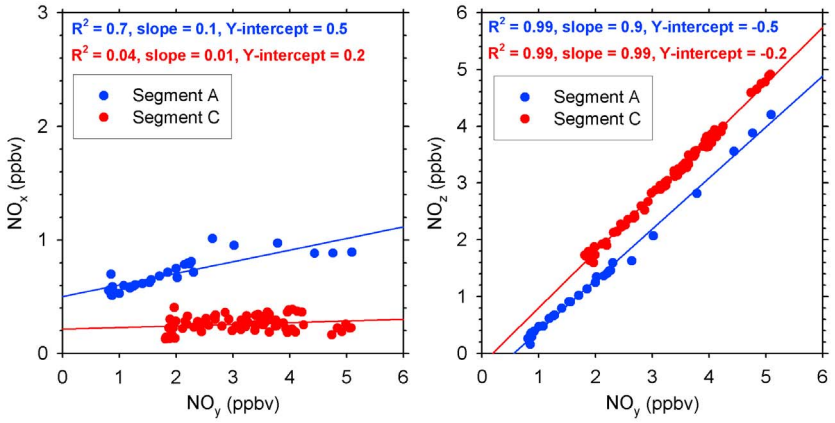

Figure 12. Scatterplots of observed NO_x and NO_z against the total NO_y for the selected plume segments in Flights A and C shown Figure 10.

to interpret the observed loss of NO_x in the Houston urban and petrochemical industrial plume. In the CPM approach a Lagrangian gas-aerosol box model is initialized using the available ground and/or aircraft observations at or near the plume emission source. The box model is then integrated forward in time, taking into account the changes in species concentrations inside the box due to emissions, gas-phase reactions, gas-particle interactions, dry deposition, and dilution along a trajectory. The predicted species concentrations are then evaluated against observations in the plume at increasing downwind distances with estimated processing times since initialization [e.g., *Zaveri et al.*, 2003, 2010].

4.1. Model Description and Inputs

[29] We use the MOSAIC (Model for Simulating Aerosol Interactions and Chemistry) aerosol model [*Zaveri et al.*, 2008] in a Lagrangian box model framework, which includes chemical reactions, dry deposition, and allows for horizontal dilution and vertical entrainment in a developing boundary layer as described by *Zaveri et al.* [2003]. MOSAIC employs comprehensive treatments for aerosol chemistry, thermodynamics (phase state and water content), dynamic gas-particle partitioning, and other microphysical processes. The gas-phase chemistry in MOSAIC is simulated with the photochemical mechanism CBM-Z [*Zaveri and Peters*, 1999], which contains all the standard trace gas reactions typically represented in air quality models. The model includes the heterogeneous hydrolysis of N_2O_5 on aerosol surfaces, with user-specified value for $\gamma(N_2O_5)$ [*Zaveri et al.*, 2010]. The gas phase reaction of N_2O_5 and H_2O was turned off in the model based on the recent determinations of the lifetime of N_2O_5 from field observations [*Brown et al.*, 2006, 2009; *Sommariva et al.*, 2008].

[30] In the present application vertical entrainment is ignored since the Houston plume segments began in the evening when turbulence in the mixed layer had dissipated. After sunset, the plume segments are in the nocturnal residual layer that is decoupled from the stable surface layer. Dry deposition and emissions are ignored for the same reason. The Lagrangian box model is initialized using the aircraft measurements at each point (1 min average; total 26 points) along the selected plume Segment A (i.e., the blue line in Figure 10) during Flight A. The initialized species include NO, NO_2, O_3, VOCs, HNO_3, PAN, ONIT, and aerosol size distribution. NO_3 radical and N_2O_5 mixing ratios were assumed to be zero since Segment A was sampled 1.5 h before sunset.

[31] PAN can decompose back to NO_2 and peroxy acyl radicals and thus serve as a reservoir of NO_x. As a result, the choice of initial PAN mixing ratios would have an impact on the predicted NO_2 mixing ratios. During the TexAQS 2000 campaign in Houston, *Roberts et al.* [2003] measured PANs, which ranged up to 6.5 ppbv and were broadly correlated with O_3, but the PAN/total NO_z ratio was not reported. An average PAN/NO_y ratio of 12% was reported in Claremont, CA [*Grosjean*, 1983] while more recent measurements in Nashville, TN, resulted in an average PAN/NO_y ratio of 10% [*Roberts et al.*, 2002]. Here we set PAN at 10% of NO_y. When initializing PAN in the model, we also initialized the corresponding acyl peroxy radicals ($RC(O)O_2$) such that they were in equilibrium with the specified PAN and the observed NO_2 mixing ratios at the observed temperature at a given point.

[32] According to the ground-based observations of *Rosen et al.* [2004] during the TexAQS 2000 campaign, up to 50% of the total NO_z in the photochemically aged Houston plume was found to be in the form of alkyl nitrates, which were well correlated with O_3. By late afternoon (1400–1800 CDT), the observed correlation between O_3 and total alkyl nitrates had a slope of 41 (R^2 = 0.74). We apply the correlation of *Rosen et al.* [2004] to initialize the total alkyl nitrates mixing ratios along plume Segment A as $[ONIT]_A = ([O_3]_A - [O_3]_{bkg})/41$, where the background $[O_3]_{bkg}$ was set at 30 ppbv. Mixing ratios of HNO_3 along plume Segment A were then estimated from mass balance as $[HNO_3]_A = [NO_z]_A - [ONIT]_A - [PAN]_A$.

[33] Initial lumped olefins (OLET) mixing ratios in the model were assumed to be the sum of the PTR-MS signals at *m/z* 43 and *m/z* 57. Initial ethene (C_2H_2) was assumed to be 2[NO_y] based on the measured emission ratios for several petrochemical complexes by *Ryerson et al.* [2003]. Acetaldehyde (CH_3CHO) mixing ratios in the model were initialized using the PTR-MS signal at *m/z* 45. Initial HCHO

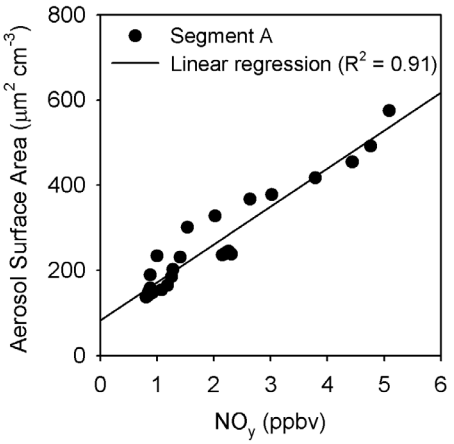

Figure 13. Scatterplot of the estimated total aerosol surface area versus NO_y along Segment A.

was assumed to be 0.8[NO_y] based on HCHO versus NO_y correlations observed downwind of the Ship Channel by *Wert et al.* [2003]. Background mixing ratios of methane and ethane were set at 1800 and 2 ppbv, respectively.

[34] As discussed earlier, *Brown et al.* [2009] had determined small values for $\gamma(N_2O_5)$ between 0.5 and 6 X 10^{-3} for aged Houston urban aerosol, of which more than 60% was composed of organic mass, and relative humidity was between 60% and 85%. Negligibly small values for $\gamma(N_2O_5)$ were also estimated for organic-rich aerosols at moderate relative humidities in other field studies [*Brown et al.*, 2006; *Zaveri et al.*, 2010]. While aerosol composition was not explicitly measured in the present study, we expect the aged Houston urban/industrial aerosol encountered during the SETTS campaign to be also dominated by organic mass. Since the RH in Segments A and C were moderate (50–65%), we assign $\gamma(N_2O_5)$ = 0.001 in this study. As mentioned earlier, the aerosol size distribution was measured only between 0.1 and 0.4 μm diameters. As a result, the corresponding aerosol surface areas (SA) along Segment A ranged between only 2 and 12 μm^2 cm^{-3}. The measured SA values were therefore scaled up by a factor of 50 to obtain the total aerosol surface area values that were comparable to those observed in Houston by *Brown et al.* [2009]. A plot of the estimated total aerosol surface area as a function of NO_y mixing ratio is shown in Figure 13.

[35] The initial concentrations and model parameter values are summarized in Table 3 and displayed in Figure 14. Case 1 is the "base case" in which all the initial concentrations and parameter values are specified as discussed above. In Case 2 the initial VOC concentrations are set to zero to examine the effects of NO_3-VOC reactions on the evolution of NO_x and various NO_z species. All other concentrations and parameter values in Case 2 are same as in the base case. Finally, Case 3 is also same as the base case, except $\gamma(N_2O_5)$ is assigned a relatively high value of 0.1 to examine the role of N_2O_5 heterogeneous hydrolysis under the given conditions.

4.2. Model Evaluation and Discussion

[36] The model was initialized using observations made along Segment A (as described above) and was integrated forward in time for 8 h along the observed trajectory as characterized by the CMET balloons. Scatterplots of various predicted species versus NO_y or CO in the "final" Segment A (i.e., 8 h later) were then compared with the observed scatterplots in Segment C (i.e., the red line in Figure 10) to evaluate the performance of the model.

4.2.1. Case 1 (Base Case)

[37] Plots for Case 1 (base case) are shown in Figure 15, which includes comparisons of scatterplots of both observed and predicted values of: NO_x versus NO_y, NO_z versus NO_y, O_3 versus CO, propene versus NO_y, and acetaldehyde versus NO_y. Figure 15 also shows scatterplots of various assumed initial and predicted final NO_z species (N_2O_5, NO_3, HNO_3, organic nitrates, and PAN) versus NO_y (note that initial mixing ratios of NO_3 and N_2O_5 are not shown as they were assumed to be zero). The model is able to reproduce the loss of NO_x and the corresponding increase in total NO_z to within ~0.2 ppbv of the observed values along Segment C. The predicted O_3 mixing ratios are 0.5 to 4 ppbv lower than the corresponding initial values due to reactions with NO_2 and olefins (propene, ethene). However, this decrease is too small to be noticeable from the scatterplot of observed O_3 versus CO along Segment C. The predicted propene mixing ratios are 0.1 to 3.5 ppbv lower than the corre-

Table 3. Initial Concentrations and Parameters for Model Sensitivity Cases

Species Name or Class	Notation	Initial Concentration (ppbv) or Parameter Value		
		Case 1 (Base Case)[a]	Case 2	Case 3
Ozone	O_3	$[O_3]_A$	Same as Case 1	Same as Case 1
Nitric oxide	NO	$[NO]_A$	Same as Case 1	Same as Case 1
Nitrogen dioxide	NO_2	$[NO_2]_A$	Same as Case 1	Same as Case 1
Peroxy acyl nitrates	PAN	$0.1[NO_y]_A$	Same as Case 1	Same as Case 1
Organic nitrates	ONIT	$([O_3]_A - 30)/41$	Same as Case 1	Same as Case 1
Nitric acid (gas + particle)	HNO_3	$[NO_z]_A - [ONIT]_A - [PAN]_A$	Same as Case 1	Same as Case 1
Lumped olefins	OLET	$[m/z\ 43]_A + [m/z\ 57]_A$	0	Same as Case 1
Acetaldehyde	CH_3CHO	$[m/z\ 45]_A$	0	Same as Case 1
Ethene	C_2H_4	$2[NO_y]_A$	0	Same as Case 1
Formaldehyde	HCHO	$0.8[NO_y]_A$	0	Same as Case 1
Methane	CH_4	1800	Same as Case 1	Same as Case 1
Ethane	C_2H_6	2	Same as Case 1	Same as Case 1
Aerosol surface area	SA	$50[SA]_A$	Same as Case 1	Same as Case 1
N_2O_5 uptake coefficient	$\gamma(N_2O_5)$	0.001	Same as Case 1	0.1

[a]Subscript A in the species concentration refers to observed or estimated mixing ratios along the plume Segment A.

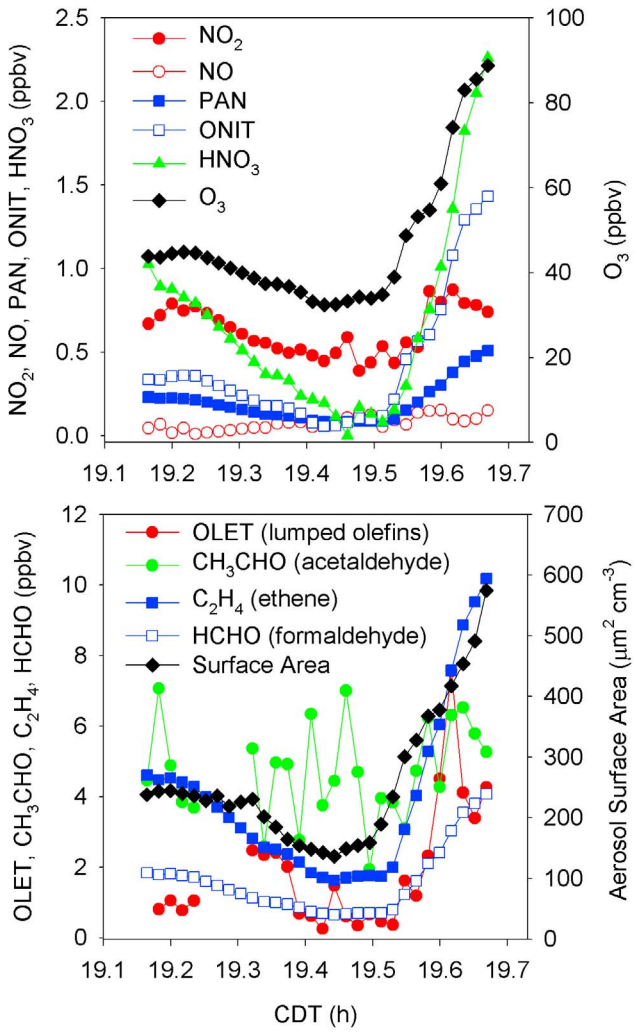

Figure 14. Observed and estimated mixing ratios of various species and estimated aerosol surface area along Segment A used to initialize the model.

sponding initial values due to its reactions with O_3 and NO_3 radicals, although similar decreases in propene mixing ratios are not seen in the scatterplot of propene versus NO_y for Segment C. Ozonolysis of propene produces acetaldehyde among other species while it is destroyed due to reaction with NO_3 radicals. As a result, the predicted acetaldehyde mixing ratios are slightly lower (~0.2 ppbv) or up to 1.5 ppbv higher than the corresponding initial values. In contrast, the observed acetaldehyde mixing ratios along Segment C were generally about 1–3 ppbv lower than the initial levels observed along Segment A. These results indicate that there were strong gradients in the propene/NO_y and acetaldehyde/NO_y ratios in the aged plume, which caused appreciable discrepancies between the initial and final mixing ratios of propene and acetaldehyde in the quasi-Lagrangian plume segments. The NO_3 radical is highly reactive with propene and acetaldehyde, with the calculated NO_3 lifetimes due to these reactions ranging between 10 and 60 min for the observed propene and acetaldehyde mixing ratios along Segment A. As a result, the predicted final NO_3 and N_2O_5 mixing ratios are small, with average values of 10.6 ± 3.6 and 2.0 ± 0.9 pptv, respectively. In contrast, the predicted HNO_3, organic nitrates, and PAN show comparable increases of up to 0.2 ppbv each, indicating that about two thirds of the NO_x lost overnight is converted into HNO_3 and stable organic nitrates while the remaining one third is converted into reservoir species such as PAN, with negligibly small amounts present as NO_3 and N_2O_5.

4.2.2. Case 2

[38] In Case 2, the reactive olefins and aldehydes (ethene, propene, formaldehyde, and acetaldehyde) were set to zero to examine the effects of NO_3-VOC reactions on the predicted NO_x, NO_z, and other species. Mixing ratios of methane and ethane were still set at their background values. As shown in Figure 16, the model does not reproduce the observed loss of NO_x and the corresponding increase in total NO_z along Segment C. In the absence of NO_3-VOC reactions, the predicted final NO_3 and N_2O_5 mixing ratios are relatively higher than the base case levels, with average values at 142 ± 32 and 36 ± 15 pptv, respectively. As expected, negligible changes in organic nitrates mixing ratios are predicted in the absence of propene. Even as NO_2 gradually reacted with O_3 to form the highly reactive NO_3 radicals, no additional $RC(O)O_2$ radicals are formed in the absence of propene and acetaldehyde. As a result, the $RC(O)O_2 + NO_2 \Leftrightarrow$ PAN equilibrium shifts to the left, causing PAN mixing ratios to decrease by up to 0.3 ppbv. At the same time the $RC(O)O_2 + NO_3$ reaction pathway serves as a source of HO_2 radicals, which leads to increase in HNO_3 by up to 0.3 ppbv via reactions (11)–(16). Loss of PAN is thus compensated by production of HNO_3, which effectively causes the NO_x and NO_z mixing ratios to change only slightly after 8 h. Case 1 and 2 results therefore illustrate the role of reactive olefins, aldehydes and PAN in the observed loss of NO_x from Segment A to C.

4.2.3. Case 3

[39] In Case 3, $\gamma(N_2O_5)$ was set at a relatively high value of 0.1 to examine its effect on the predicted evolution of NO_x and NO_z. As shown in Figure 17, the model is able to reproduce the loss of NO_x and the corresponding increase in total NO_z to within 0.1 ppbv of the observed values along Segment C, which is an improvement over the base case results. The predicted HNO_3 mixing ratio increases by up to 0.5 ppbv while organic nitrates and PAN show comparable increases of up to ~0.15 ppbv each. Thus, about two thirds of the NO_x lost in Segment A is converted into HNO_3 while the remaining one third is converted into organic nitrates and PAN. As discussed earlier, $\gamma(N_2O_5)$ is likely on the order of 0.001 for Houston urban/industrial aerosol since a significant fraction of the aerosol would be composed of organic species [*Brown et al.*, 2009], although it is not possible to rule out a higher value of $\gamma(N_2O_5)$ in this particular study due to lack to direct measurements of NO_3, N_2O_5, HNO_3, and aerosol composition. In either case, it appears that NO_x could not have been completely converted to HNO_3.

[40] *Luria et al.* [2008] found near 100% conversion of NO_x to NO_z overnight for the 21 July episode, but attributed it entirely to formation of HNO_3 via reaction of NO_3 radical with saturated hydrocarbons and hydrolysis of N_2O_5 under humid conditions. Reactions of NO_3 with saturated hydrocarbons are typically 2 orders of magnitude slower than with olefins [*Atkinson*, 1994], and as mentioned above, hydro-

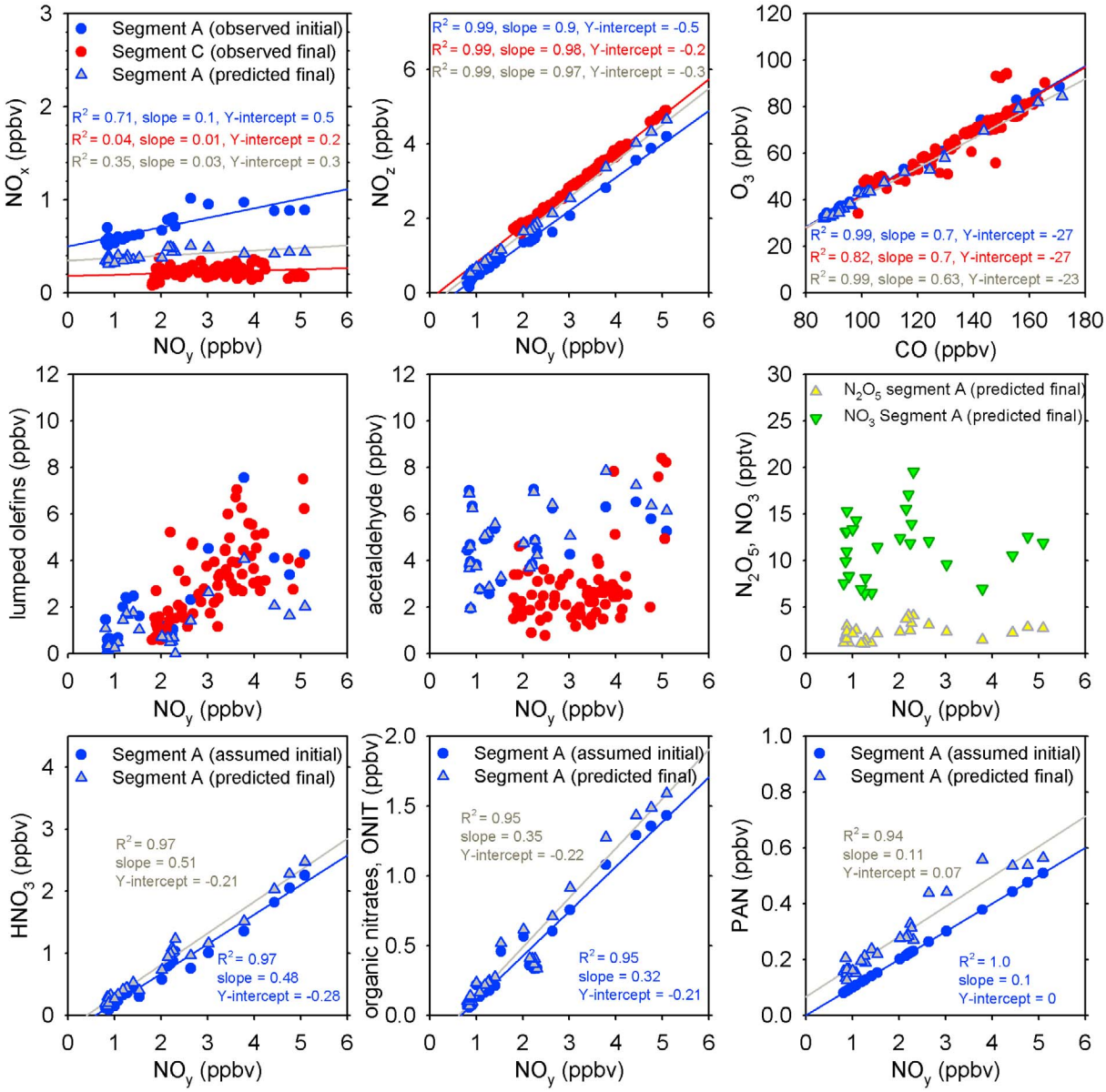

Figure 15. Case 1 (base case) results. Scatterplots of NO_x versus NO_y, NO_z versus NO_y, O_3 versus CO, lumped olefins versus NO_y, acetaldehyde versus NO_y, N_2O_5 and NO_3 versus NO_y, HNO_3 versus NO_y, organic nitrates versus NO_y, and PAN versus NO_y. Observations and estimations are shown with solid circles, and model predictions are shown with triangles. Lines are linear regression fits.

lysis of N_2O_5 is expected to be rather slow in the presence of organic aerosol. Thus, while the near 100% conversion of NO_x to NO_z observed for the 21 July episode is in excellent agreement with the observations for the 26 July episode (this work), the mechanistic explanations offered by *Luria et al.* [2008] appear to be inconsistent with the present analysis.

4.2.4. Potential Impact on Next Day Photochemistry

[41] Assuming the base case (i.e., case 1) simulation effectively represents the overnight transport and chemical processing of O_3, NO_y, and VOC species in the photochemically aged Houston plume, we briefly extend the analysis here to investigate the potential impact of such a plume on photochemical O_3 production the next day. We note that this is not an exhaustive analysis and that the results shown here should be used with caution because of the following assumptions made in initializing and running the model: (1) fresh emissions and plume dilution in the residual layer were neglected for the nighttime period (as was done in Case 1) and during the following daytime period as well, and (2) the list of VOCs used to initialize the model does not include aromatics, alkanes, and other species, which may have been present in the plume but were either not detected or measured.

[42] We focus our attention on one representative sample near the peak NO_y levels in Segment A. Figure 18 shows the predicted evolution of various species in the selected

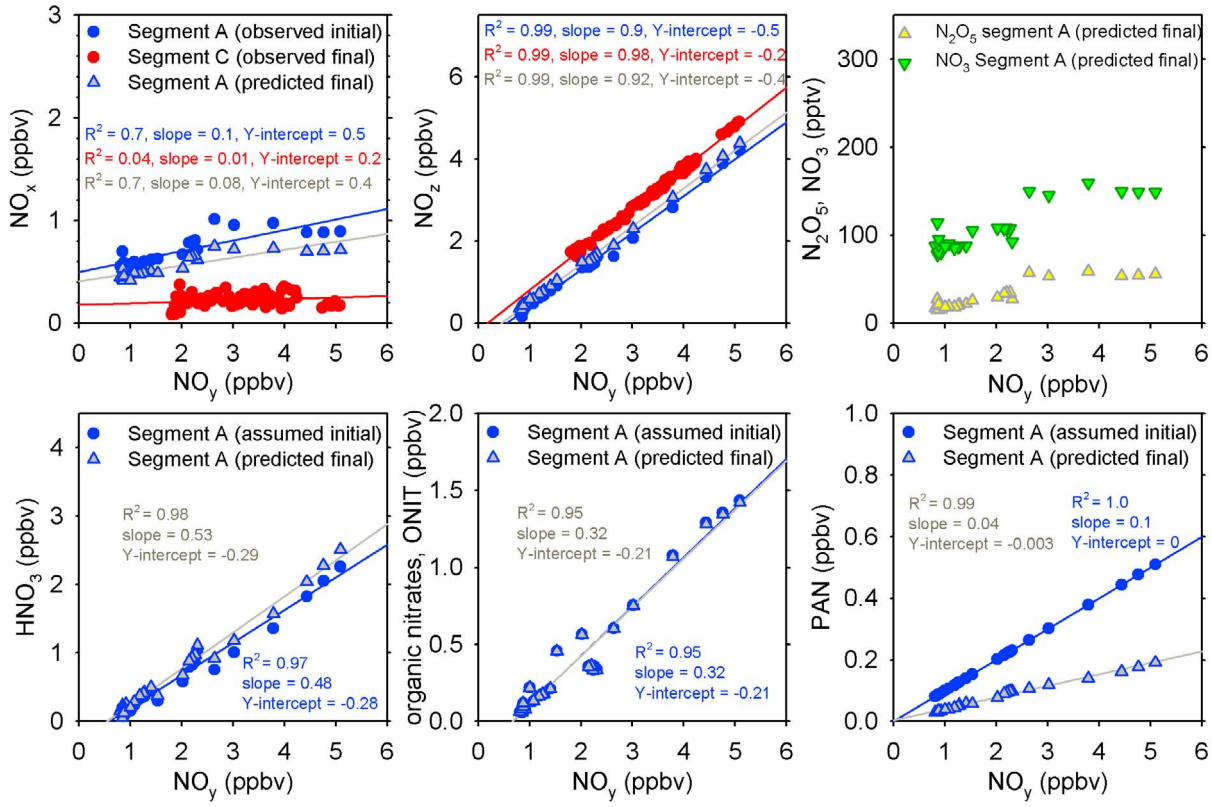

Figure 16. Case 2 results. Scatterplots of NO_x versus NO_y, NO_z versus NO_y, N_2O_5 and NO_3 versus NO_y, HNO_3 versus NO_y, organic nitrates versus NO_y, and PAN versus NO_y. Observations and estimations are shown with solid circles, and model predictions are shown with triangles. Lines are linear regression fits.

sample air parcel as it is advected downwind for 24 h (from 1935 CDT 26 July through 1935 CDT 27 July). Reactions with olefins and NO_2 caused the O_3 mixing ratio to decrease steadily from the initial value of about 83 ppbv around sunset to its minimum at 78 ppbv by sunrise (0637 CDT) the next day. Likewise, NO_2, propene, and ethene mixing ratios decreased from 0.8 to 0.35 ppbv, 4 to 1.6 ppbv, and 8.8 to 7.6 ppbv, respectively, by sunrise while total NO_z increased from 3.5 to 4 ppbv due to steady increases in HNO_3 and organic nitrates mixing ratios from NO_3+VOC reactions. Continued production of $RC(O)O_2$ radicals from acetaldehyde + NO_3 reaction caused the PAN mixing ratio to experience a local maximum around midnight, followed by a steady decline until sunrise due to continued loss of NO_2. Oxidation of propene and ethene caused acetaldehyde and formaldehyde mixing ratios to also steadily increase from their respective initial values of 6.5 and 3.5 ppbv to their respective peak values of 7.4 and 6.8 ppbv by 0730 CDT. Nighttime mixing ratios of OH and HO_2 radicals were about 0.006 and 6 pptv, respectively, with primary sources being oxidation of VOCs (olefins and aldehydes) and the ensuing radical chemistry. Nighttime mixing ratios of N_2O_5 and NO_3 radicals were rather small at about 3 and 10 pptv, respectively.

[43] After sunrise, the OH and HO_2 radicals rapidly increased and experienced their peak values between 1200 CDT and 1500 CDT. Mixing ratios of NO_2, olefins, and aldehydes rapidly decreased during this period due to photolysis and/or oxidation by OH radicals. Organic nitrates experienced a slow decline as its loss due to photolysis and oxidation by OH radicals was partially compensated by its formation from reaction of the resulting nitratoalkyl peroxy (NAP) radicals with NO. Mixing ratio of PAN experienced another local maximum around noon due to increased production of $RC(O)O_2$ radicals from acetaldehyde and propene oxidation until shortly thereafter. Interestingly, photochemical production of O_3 after sunrise brought its mixing ratio back to its previous day's value by sunset, with no net production or loss.

[44] The photochemically aged Houston plume would be significantly depleted in NO_x by next morning, but may still contain appreciable levels of reactive VOCs. Photochemical ozone formation in such a plume would be highly sensitive to fresh emissions of NO_x. For instance, a rather modest increase in NO_x mixing ratio of 2 ppbv in the aged plume at 0900 CDT the next day due to fresh emissions would produce 25 ppbv additional O_3 by 1800 CDT. Dilution would tend to reduce the peak O_3 levels in the plume, but contribute to regional background O_3. Finally, while comprehensive aerosol measurements were not made during this study, organic nitrates formed via NO_3 reactions with olefins can potentially contribute to secondary organic aerosol formation at night [*Barnes et al.*, 1990; *Shepson et al.*, 1996; *Starn et al.*, 1998; *Ng et al.*, 2008; *Zaveri et al.*, 2010].

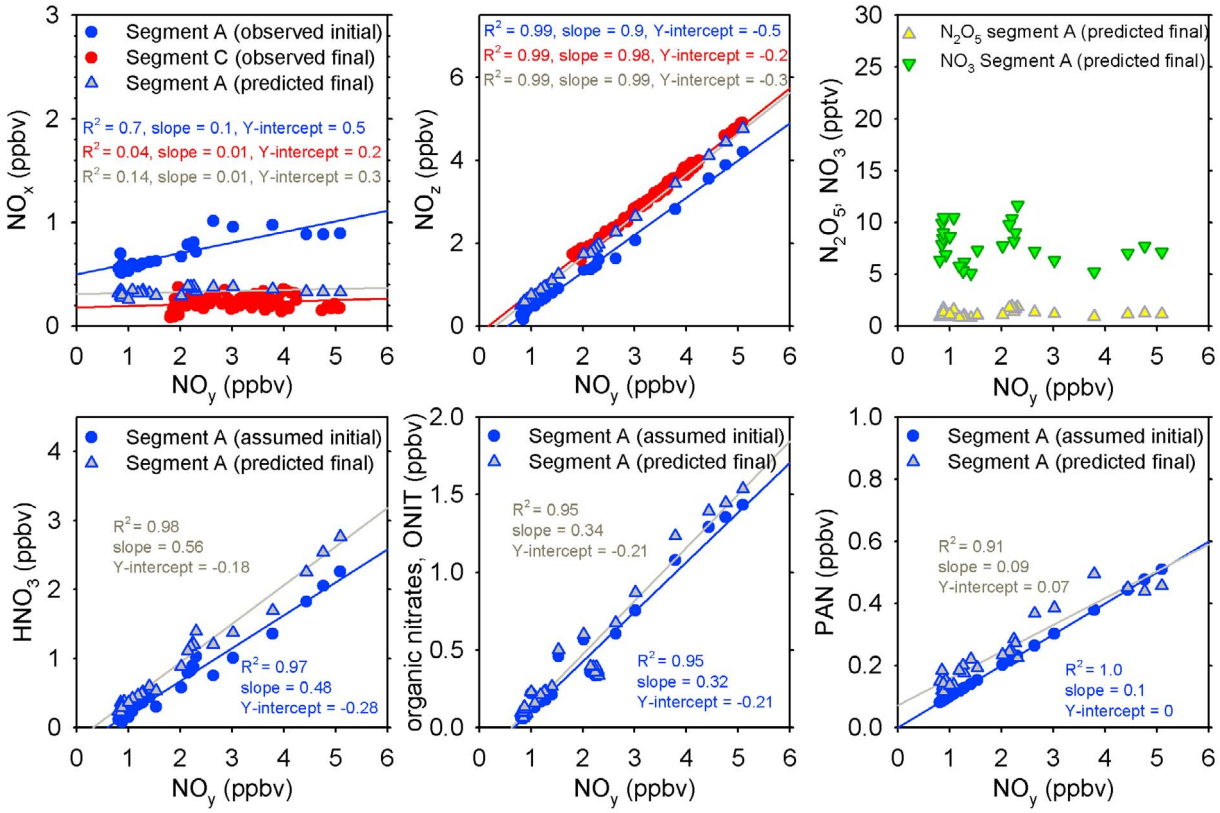

Figure 17. Case 3 results. Scatterplots of NO_x versus NO_y, NO_z versus NO_y, N_2O_5 and NO_3 versus NO_y, HNO_3 versus NO_y, organic nitrates versus NO_y, and PAN versus NO_y. Observations and estimations are shown with solid circles and model predictions are shown with triangles. Lines are linear regression fits.

Additional observations and modeling studies are necessary to assess the impact of aged urban/industrial plumes on regional ozone and aerosol levels over multiple days.

5. Summary and Conclusions

[45] In July 2005, an aircraft campaign was carried out to investigate the nighttime chemical processing and dispersion of photochemically aged Houston urban and petrochemical industrial pollution plumes containing high levels of aerosols, O_3, CO, volatile organic compounds (VOCs), total odd nitrogen compounds (NO_y), and relatively small amounts of unreacted NO_x. An instrumented Twin Otter aircraft was deployed to measure CO, O_3, NO_x, NO_y, hydrocarbons (PTR-MS), and aerosol size distribution (0.1–0.4 μm). An improved quasi-Lagrangian aircraft sampling strategy, aided by the newly developed controlled meteorological (CMET) balloons, was successfully used to monitor the nighttime transport and chemical transformation of the Houston plume as it drifted across the state of Texas.

[46] We have reported here on the analysis of the 26 July episode. A photochemically aged plume containing a mixture of urban and petrochemical industrial emissions was located north of Houston metropolitan area under southerly flow conditions. Aircraft vertical profiles showed the plume to be well-mixed to 1600 m MSL. This plume was tagged with a pair of CMET balloons at sunset and tracked for ~300 km over 8 h into north Texas. One of the two CMET balloons was programmed to make repeated soundings of in situ temperature, moisture, wind velocity, and pressure, while the other balloon, also measuring these variables, was flown in the constant-altitude mode at approximately 600 m MSL. The quasi-Lagrangian balloon soundings provided a unique view of the evolving in situ structure of the atmosphere. The positions of both balloons were received onboard the aircraft via satellite communications to guide the aircraft transects within the tagged urban plume segment at increasing downwind distances and processing times.

[47] CMET balloon soundings and trajectory data showed that the Houston plume experienced appreciable shearing due to the development of a low-altitude nocturnal jet between 300 and 500 m MSL. However, aircraft measurements indicated that the plume in the residual layer above 600 m MSL remained undiluted even after 8 h and 300 km of transport due to lack of turbulent mixing above the jet. Enhanced levels of olefins (dominated by propene) and acetaldehyde of petrochemical industrial origin were observed in this plume at sunset and 8 h later, and analysis of quasi-Lagrangian aircraft data yielded evidence for 40–60% conversion of NO_x to NO_z in the plume over this period.

[48] A constrained plume modeling (CPM) analysis of the quasi-Lagrangian data was performed using the comprehensive gas-aerosol chemistry box model MOSAIC (Model

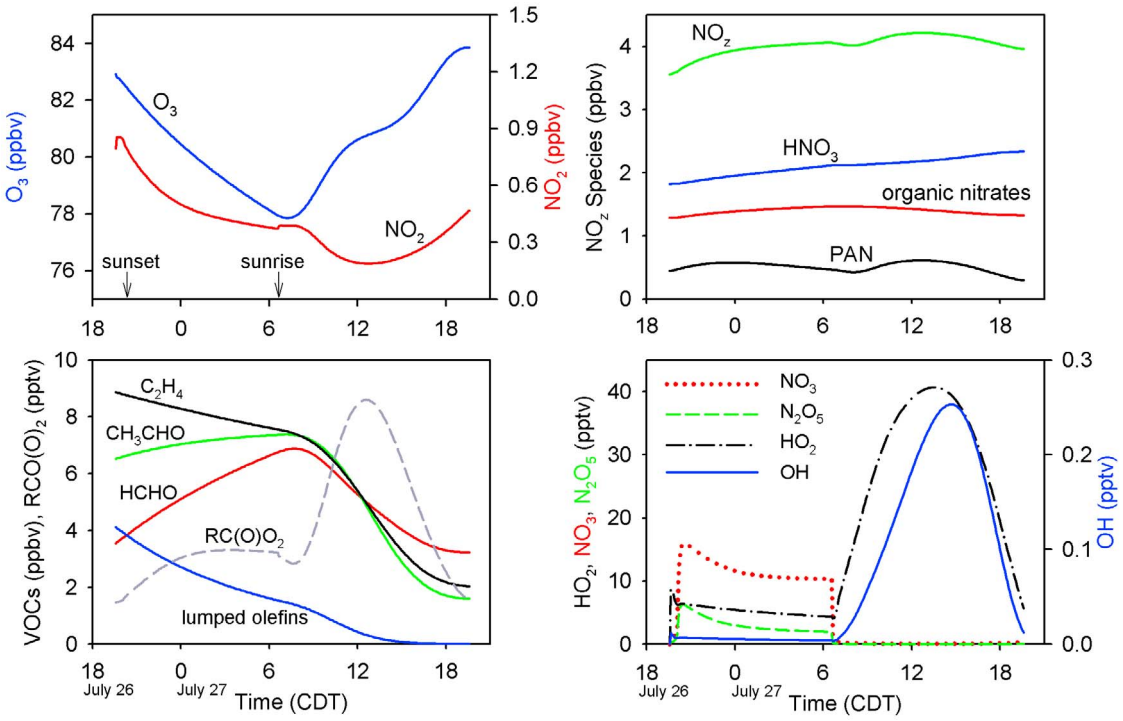

Figure 18. Evolution of various species as a function of processing time for a representative sample in Segment A for Case 1 (base case) conditions.

for Simulating Aerosol Interactions and Chemistry). The model was able to reproduce the observed overnight depletion of small amounts of NO_x (<1 ppbv) present in the photochemically aged plume at sunset, and showed that it was converted to roughly equal amounts of nitric acid, organic nitrates, and peroxy acyl nitrates via reactions of NO_3 radicals with olefins and aldehydes and the ensuing radical chemistry at night. The predicted NO_3 and N_2O_5 mixing ratios were quite small at about 10 and 3 pptv, respectively, indicating fast loss of NO_3 due to its reactions with VOCs. The N_2O_5 heterogeneous uptake coefficient $\gamma(N_2O_5)$ was likely on the order of 0.001 for Houston urban/industrial aerosol since a significant fraction of the aerosol would be composed of organic species [*Brown et al.*, 2009], although it was not possible to rule out a higher value of $\gamma(N_2O_5)$ in this particular study due to lack to direct measurements of NO_3, N_2O_5, and HNO_3.

[49] The overnight transport of aged but concentrated urban and industrial plumes containing substantial amounts of reactive VOCs, various NO_z species (nitric acid, organic nitrates, and peroxy acyl nitrates), and aerosols can potentially affect the air quality in regions several hundred kilometers downwind the next day. Organic nitrates formed via NO_3 reactions with olefins can potentially contribute to secondary organic aerosol formation in such concentrated urban/petrochemical industrial plumes as they are transported overnight. However, nighttime SOA formation could not be investigated since aerosol composition was not characterized in this field study. Substantial amounts of ozone could also form in such VOC-rich plumes when mixed with even modest amounts of freshly emitted NO_x in the downwind regions the next day.

[50] Much remains to be learned about nighttime chemistry, the role of heterogeneous reactions on aerosols, and the overnight transport and dispersion of photochemically aged plumes in the nocturnal residual layer. Further field measurements and modeling studies to investigate nighttime evolution of aerosols and evaluate the impact of aged urban and industrial plumes on regional ozone and aerosol levels should be of considerable future interest.

[51] **Acknowledgments.** We thank the three anonymous reviewers for their detailed and thoughtful comments on the manuscript. We gratefully acknowledge the support of Texas Environmental Research Consortium (TERC), Houston Advanced Research Center (HARC), and Texas Commission on Environmental Quality (TCEQ) during 2005 for the SETTS field campaign and during 2008–2009 for the analysis of the data. Partial support was also provided by the DOE Atmospheric System Research (ASR) Program. We are also grateful to Brian Wing and the staff at Wing Aviation at the Lone Star Executive airport in Conroe, Texas, for hosting us. We thank Scott Seibold of Twin Otter International and the pilots, Bill Clark and Cathy Todoverto, for translating our scientific goals into safe and flawless missions. Finally, we are most grateful to Jay Olaguer and Alex Cuclis at HARC and Doug Boyer and Ken Rozacky at TCEQ for their support and guidance throughout this project. PNNL is operated for the U.S. Department of Energy by Battelle Memorial Institute under contract DE-AC06-76RLO 1830.

References

Angell, J. K., C. R. Dickson, and W. H. Hoecker Jr. (1976), Tetroon trajectories in the Los Angeles basin defining the source of air reaching the San Bernadino-Riverside area in late afternoon, *J. Appl. Meteorol.*, *15*(3), 197–204, doi:10.1175/1520-0450(1976)015<0197:TTITLA>2.0.CO;2.

Atkinson, R. (1994), Gas-phase tropospheric chemistry of organic compounds: A review, *J. Phys. Chem. Ref. Data Monogr.*, *2*, 1–216.

Badger, C. L., P. T. Griffiths, I. George, J. P. D. Abbatt, and R. A. Cox (2006), Reactive uptake of N_2O_5 by aerosol particles containing mixtures of humic acid and ammonium sulfate, *J. Phys. Chem. A*, *110*, 6986–6994, doi:10.1021/jp0562678.

Barnes, I., V. Bastian, K. H. Becker, and Z. Tong (1990), Kinetics and products of the reactions of NO_3 with monoalkenes, dialkenes, and monoterpenes, *J. Phys. Chem.*, *94*, 2413–2419, doi:10.1021/j100369a041.

Bertram, T. H., and J. A. Thornton (2009), Toward a general parameterization of N_2O_5 reactivity on aqueous particles: The competing effects of particle liquid water, nitrate and chloride, *Atmos. Chem. Phys.*, *9*, 8351–8363.

Brown, S. S., H. Stark, T. B. Ryerson, E. J. Williams, D. K. Nicks Jr., M. Trainer, F. C. Fehsenfeld, and A. R. Ravishankara (2003), Nitrogen oxides in the nocturnal boundary layer: Simultaneous in situ measurements of NO_3, N_2O_5, NO_2, NO, and O_3, *J. Geophys. Res.*, *108*(D9), 4299, doi:10.1029/2002JD002917.

Brown, S. S., et al. (2006), Variability in nocturnal nitrogen oxide processing and its role in regional air quality, *Science*, *311*, 67–70, doi:10.1126/science.1120120.

Brown, S. S., et al. (2009), Reactive uptake coefficients for N_2O_5 determined from aircraft measurements during the Second Texas Air Quality Study: Comparison to current model parameterizations, *J. Geophys. Res.*, *114*, D00F10, doi:10.1029/2008JD011679.

Daum, P. H., L. I. Kleinman, S. R. Springston, L. J. Nunnermacker, Y.-N. Lee, J. Weinstein-Lloyd, J. Zheng, and C. M. Berkowitz (2004), Origin and properties of plumes of high ozone observed during the Texas 2000 Air Quality Study (TexAQS 2000), *J. Geophys. Res.*, *109*, D17306, doi:10.1029/2003JD004311.

de Gouw, J. A., C. Warneke, T. Karl, G. Eerdekens, C. van der Veen, and R. Fall (2003), Sensitivity and specificity of atmospheric trace gas detection by proton-transfer-reaction mass spectrometry, *Int. J. Mass Spectrom.*, *223–224*, 365, doi:10.1016/S1387-3806(02)00926-0.

Fall, R., T. Karl, A. Jordan, and W. Lindinger (2001), Biogenic C5 VOCs: Release from leaves after freeze-thaw wounding and occurrence in air at a high mountain observatory, *Atmos. Environ.*, *35*, 3905, doi:10.1016/S1352-2310(01)00141-8.

Folkers, M., T. F. Mentel, and A. Wahner (2003), Influence of an organic coating on the reactivity of aqueous aerosols probed by the heterogeneous hydrolysis of N_2O_5, *Geophys. Res. Lett.*, *30*(12), 1644, doi:10.1029/2003GL017168.

Fortner, E. C., J. Zheng, R. Zhang, W. B. Knighton, R. W. Volkamer, P. Sheehy, L. Molina, and M. Andre (2009), Measurements of volatile organic compounds using proton transfer reaction-mass spectrometry during the MILAGRO 2006 campaign, *Atmos. Phys. Chem.*, *9*(2), 467–481.

Gilman, J. B., et al. (2009), Measurements of volatile organic compounds during the 2006 TexAQS/GoMACCS campaign: Industrial influences, regional characteristics, and diurnal dependencies of the OH reactivity, *J. Geophys. Res.*, *114*, D00F06, doi:10.1029/2008JD011525.

Grosjean, D. (1983), Distribution of atmospheric nitrogenous pollutants at a Los Angeles area smog receptor site, *Environ. Sci. Technol.*, *17*, 13–19, doi:10.1021/es00107a006.

Hansel, A., A. Jordan, R. Holzinger, P. Prazeller, W. Vogel, and W. Lindinger (1995), Proton-transfer reaction mass-spectrometry—Online trace gas-analysis at the ppb level, *Int. J. Mass Spectrom.*, *149*, 609–619.

Jacob, D. (2000), Heterogeneous chemistry and tropospheric ozone, *Atmos. Environ.*, *34*, 2131–2159.

Jiang, G., and J. D. Fast (2004), Modeling the effects of VOC and NO_x emission sources on ozone formation in Houston during the TexAQS 2000 Field Campaign, *Atmos. Environ.*, *38*, 5071–5085.

Jobson, B. T., C. M. Berkowitz, W. C. Kuster, P. D. Goldan, E. J. Williams, F. C. Fesenfeld, E. C. Apel, T. Karl, W. A. Lonneman, and D. Riemer (2004), Hydrocarbon source signatures in Houston, Texas: Influence of the petrochemical industry, *J. Geophys. Res.*, *109*, D24305, doi:10.1029/2004JD004887.

Johnson, D. W., et al. (2000), An overview of the Lagrangian experiments undertaken during the North Atlantic Regional Aerosol Characterization Experiment (ACE-2), *Tellus, Ser. B*, *52*, 290–320.

Lindinger, W., A. Hansel, and A. Jordan (1998), On-line monitoring of volatile organic compounds at pptv levels by means of proton-transfer-reaction mass spectrometry (PTR-MS)—Medical applications, food control and environmental research, *Int. J. Mass. Spectrom.*, *173*, 191–241.

Karl, T., T. Jobson, W. C. Kuster, E. Williams, J. Stutz, R. Shetter, S. R. Hall, P. Goldan, F. Fehsenfeld, and W. Lindinger (2003), Use of proton-transfer-reaction mass spectrometry to characterize volatile organic compound sources at the La Porte super site during the Texas Air Quality Study 2000, *J. Geophys. Res.*, *108*(D16), 4508, doi:10.1029/2002JD003333.

Kleinman, L. I., P. H. Daum, Y.-N. Lee, L. J. Nunnermacker, S. R. Springston, J. Weinstein-Lloyd, and J. Rudolph (2005), A comparative study of ozone production in five U.S. metropolitan areas, *J. Geophys. Res.*, *110*, D02301, doi:10.1029/2004JD005096.

Kuster, W. C., B. T. Jobson, T. Karl, D. Riemer, E. Apel, P. D. Goldan, and F. Fehsenfeld (2004), Intercomparison of volatile organic carbon measurement techniques and data at La Porte during the TexAQS2000 air quality study, *Environ. Sci. Technol.*, *38*, 221–228, doi:10.1021/es034710r.

Luria, M., R. J. Valente, N. V. Gillani, R. L. Tanner, R. E. Imhoff, and J. F. Meagher (1999), The evolution of photochemical smog in a power plant plume, *Atmos. Environ.*, *33*, 3023–3036, doi:10.1016/S1352-2310(99)00072-2.

Luria, M., R. L. Tanner, R. J. Valente, and R. E. Imhoff (2000), The influence of natural hydrocarbons on ozone formation in an isolated power plant plume, *J. Geophys. Res.*, *105*, 9177–9188, doi:10.1029/1999JD901018.

Luria, M., R. J. Valente, S. Bairai, W. J. Parkhurst, and R. L. Tanner (2008), Nighttime chemistry in the Houston urban plume, *Atmos. Environ.*, *42*, 7544–7552, doi:10.1016/j.atmosenv.2008.04.054.

McNeill, V. F., J. Patterson, G. M. Wolfe, and J. A. Thornton (2006), The effect of varying levels of surfactant on the reactive uptake of N_2O_5 to aqueous aerosol, *Atmos. Chem. Phys.*, *6*, 1635–1644.

Ng, N. L., et al. (2008), Secondary organic aerosol (SOA) formation from reaction of isoprene with nitrate radicals (NO_3), *Atmos. Chem. Phys.*, *8*, 4117–4140, doi:10.5194/acp-8-4117-2008.

Reisinger, L. M., and S. F. Mueller (1983), Comparisons of tetroon and computed trajectories, *J. Clim. Appl. Meteorol.*, *22*, 664–672, doi:10.1175/1520-0450(1983)022<0664:COTACT>2.0.CO;2.

Riddle, E. E., P. B. Voss, A. Stohl, D. Holcomb, D. Maczka, K. Washburn, and R. W. Talbot (2006), Trajectory model validation using newly developed altitude-controlled balloons during the International Consortium for Atmospheric Research on Transport and Transformations 2004 campaign, *J. Geophys. Res.*, *111*, D23S57, doi:10.1029/2006JD007456.

Roberts, J. M., F. Flocke, C. A. Stroud, D. Hereid, E. Williams, F. Fehsenfeld, W. Brune, M. Martinez, and H. Harder (2002), Ground-based measurements of peroxycarboxylic nitric anhydrides (PANs) during the 1999 Southern Oxidants Study Nashville Intensive, *J. Geophys. Res.*, *107*(D21), 4554, doi:10.1029/2001JD000947.

Roberts, J. M., et al. (2003), An examination of the chemistry of peroxycarboxylic nitric anhydrides and related volatile organic compounds during Texas Air Quality Study 2000 using ground-based measurements, *J. Geophys. Res.*, *108*(D16), 4495, doi:10.1029/2003JD003383.

Rogers, T. M., et al. (2006), On-road measurements of volatile organic compounds in the Mexico City metropolitan area using proton transfer reaction mass spectrometry, *Int. J. Mass Spectrom.*, *252*, 26–37, doi:10.1016/j.ijms.2006.01.027.

Rosen, R. S., E. C. Wood, P. J. Wooldridge, J. A. Thornton, D. A. Day, W. Kuster, E. J. Williams, B. T. Jobson, and R. C. Cohen (2004), Observations of total alkyl nitrates during Texas Air Quality Study 2000: Implications for O_3 and alkyl nitrate photochemistry, *J. Geophys. Res.*, *109*, D07303, doi:10.1029/2003JD004227.

Ryerson, T. B., et al. (2003), Effect of petrochemical industrial emissions of reactive alkenes and NO_x on tropospheric ozone formation in Houston, Texas, *J. Geophys. Res.*, *108*(D8), 4249, doi:10.1029/2002JD003070.

Shepson, P. B., E. Mackay, and K. Muthuramu (1996), Henry's law constants and removal processes for several atmospheric beta-hydroxy alkyl nitrates, *Environ. Sci. Technol.*, *30*, 3618–3623, doi:10.1021/es960538y.

Sommariva, R., et al. (2008), Radicals in the marine boundary layer during NEAQS 2004: A model study of day-time and night-time sources and sinks, *Atmos. Chem. Phys. Discuss.*, *8*, 16,643–16,692, doi:10.5194/acpd-8-16643-2008.

Starn, T. K., P. B. Shepson, S. B. Bertman, D. D. Riemer, R. G. Zika, and K. Olszyna (1998), Nighttime isoprene chemistry at an urban-impacted forest site, *J. Geophys. Res.*, *103*, 22,437–22,447, doi:10.1029/98JD01201.

Stull, R. B. (1988), *An Introduction to Boundary Layer Meteorology*, 666 pp., Kluwer Acad., Norwell, Mass.

Suhre, K., et al. (1998), Physico-chemical modeling of the First Aerosol Characterization Experiment (ACE-1) Lagrangian B. 1: A moving column approach, *J. Geophys. Res.*, *103*, 16,433–16,456, doi:10.1029/98JD00821.

Tanner, R. L., R. J. Valente, and J. F. Meagher (1998), Measuring inorganic nitrate species with short time resolution from an aircraft platform by dual-channel ozone chemiluminescence, *J. Geophys. Res.*, *103*, 22,387–22,395, doi:10.1029/98JD00110.

Thornton, J. A., and J. P. D. Abbatt (2005), N_2O_5 reaction on submicron sea salt aerosol: Kinetics, products, and the effect of surface active organics, *J. Phys. Chem.*, *109*, 10,004–10,012.

Thornton, J. A., C. F. Braban, and J. P. D. Abbatt (2003), N_2O_5 hydrolysis on sub-micron organic aerosols: The effect of relative humidity, particle phase, and particle size, *Phys. Chem. Chem. Phys.*, *5*, 4593–4603.

Valente, R. J., R. E. Imhoff, R. L. Tanner, J. F. Meagher, P. H. Daum, R. M. Hardesty, R. V. Banta, R. J. Alvarez, R. McNider, and N. V. Gillani (1998), Ozone production during an urban air stagnation episode over Nashville, Tennessee, *J. Geophys. Res.*, *103*, 22,555–22,568, doi:10.1029/98JD01641.

Voss, P. B., E. E. Riddle, and M. S. Smith (2005), Altitude control of long-duration balloons, *J. Aircr.*, *42*(2), 478–482, doi:10.2514/1.7481.

Warneke, C., J. A. De Gouw, W. C. Kuster, P. D. Goldan, and R. Fall (2003), Validation of atmospheric VOC measurements by proton-transfer-reaction mass spectrometry using a gas chromatographic pre-separation method, *Environ. Sci. Technol.*, *37*, 2494–2501, doi:10.1021/es026266i.

Wert, B. P., et al. (2003), Signatures of terminal alkene oxidation in airborne formaldehyde measurements during TexAQS 2000, *J. Geophys. Res.*, *108*(D3), 4104, doi:10.1029/2002JD002502.

Zak, B. D. (1981), Lagrangian measurements of sulfur dioxide to sulfate conversion rates, *Atmos. Environ.*, *15*, 2583–2591, doi:10.1016/0004-6981(81)90075-5.

Zaveri, R. A., and L. K. Peters (1999), A new lumped structure photochemical mechanism for large-scale applications, *J. Geophys. Res.*, *104*, 30,387–30,415, doi:10.1029/1999JD900876.

Zaveri, R. A., C. M. Berkowitz, L. I. Kleinman, S. R. Springston, P. V. Doskey, W. A. Lonneman, and C. W. Spicer (2003), Ozone production efficiency and NO_x depletion in an urban plume: Interpretation of field observations and implications for evaluating O_3-NO_x-VOC sensitivity, *J. Geophys. Res.*, *108*(D14), 4436, doi:10.1029/2002JD003144.

Zaveri, R. A., R. C. Easter, J. D. Fast, and L. K. Peters (2008), Model for Simulating Aerosol Interactions and Chemistry (MOSAIC), *J. Geophys. Res.*, *113*, D13204, doi:10.1029/2007JD008782.

Zaveri, R. A., et al. (2010), Nighttime chemical evolution of aerosol and trace gases in a power plant plume: Implications for secondary organic nitrate and organosulfate aerosol formation, NO_3 radical chemistry, and N_2O_5 heterogeneous hydrolysis, *J. Geophys. Res.*, *115*, D12304, doi:10.1029/2009JD013250.

Zhuang, L., and B. J. Huebert (1996), A Lagrangian analysis of the total ammonia budget during ASTEX/MAGE, *J. Geophys. Res.*, *101*, 4341–4350, doi:10.1029/95JD02467.

L. Baran, Department of Atmospheric Science, University of Wyoming, 1000 E. University Ave., Laramie, WY 82071, USA.

C. M. Berkowitz and R. A. Zaveri, Atmospheric Sciences and Global Change Division, Pacific Northwest National Laboratory, MSIN K9-30, PO Box 999, Richland, WA 99352, USA. (rahul.zaveri@pnl.gov)

E. Fortner, Aerodyne Research, Inc., Billerica, MA 01821, USA.

T. P. Hartley, Department of Electrical and Computer Engineering, University of Massachusetts, 100 Natural Resources Rd., 201 Marcus Hall, Amherst, MA 01003, USA.

D. Holcomb, Electrical Engineering and Computer Sciences Department, University of California, Berkeley, 253 Cory Hall, Berkeley, CA 94720, USA.

R. L. Tanner and R. J. Valente, Environmental Technologies Department, Tennessee Valley Authority, PO Box 1010, Muscle Shoals, AL 35662, USA.

P. B. Voss, Picker Engineering Program, Smith College, 51 College Ln., Northampton, MA 01063, USA.

R. Zhang and J. Zheng, Department of Atmospheric Sciences, Texas A&M University, MS 3150, College Station, TX 77843, USA.